Investigating the Structure Directing Properties of Designer 1,8-Naphthalimide and Amphiphilic Sulfonate Anions and their Fe^{III} Thiosemicarbazone Complexes

Anthony B. Carter[†], Robert J. Laverick[†], Dominic J. Wales[†], Sarah O. Akponasa[†], Aaron J. Scott[†], Tony D. Keene[‡] and Jonathan A. Kitchen[†]*

[†] *Chemistry, University of Southampton, Southampton, SO17 1BJ, UK.*

[‡] *School of Chemistry, University College Dublin, Belfield, Dublin 4, Ireland*

Supramolecular, anions, structure-directing, 1,8-naphthalimides, iron(III), Langmuir-Blodgett

ABSTRACT: The Fe^{III} thiosemicarbazone complexes of five organic sulfonate based anions are reported {[Fe($\mathbf{L_1}$)$_2$](**X**), where $\mathbf{L_1}$ = acetylthiazole 4-phenylthiosemicarbazone and **X** = *N*-(*p*-aminobenzenesulfonate)-1,8-naphthalimide (**1**), *N*-(*m*-aminobenzenesulfonate)-1,8-naphthalimide (**2**), *N*-(5-amino-1-naphthalenesulfonate)-1,8-naphthalimide (**3**), *N*-(5-amino-2-naphthalenesulfonate)-1,8-naphthalimide (**4**) and hexadecylsulfonate (**5**)}. Four complexes feature 1,8-naphthalimide based anions, known for their structure directing properties through π-

based interactions and one complex features a long chain sulfonate anion to introduce amphiphilicity to the complex to allow formation of Langmuir-Blodgett films. A full structural and photophysical study is reported for naphthalimide based anions **1** – **4** and complexes [Fe($\mathbf{L_1}$)$_2$](**1-4**), and a structural and Langmuir study is reported for [Fe($\mathbf{L_1}$)$_2$](**5**).

INTRODUCTION

The development of functional metallosupramolecular materials is an active area of research, particularly in the fields of sensor development, catalysis, and magnetism.[1-6] The preparation of such supramolecular materials often relies on controlling and understanding weak intermolecular interactions in both the solution and the solid states.[7-10] Introducing functional groups into a system that have particular structure directing properties is one method that researchers have been using to control the overall architecture and topology of functional systems. Such "directed assembly" allows for functional metal complexes to be organised into macroscopic materials (*e.g.* MOF formation or porous coordination polymers) or immobilised onto surfaces (*e.g.* through Langmuir Blodgett (LB) deposition).[11-20] Typically, this is through inclusion of structure directing groups (SDGs) into the ligand used for coordination, however it is also possible to include such structure directing properties through the use of designer counter ions.[21-24]

Structure directing groups can take a variety of forms, including those that act as secondary building units (SBUs) and give interesting packing/ordering in the solid state; those that allow for ordered assembly on a surface; and those that allow for immobilisation into an external matrix (*e.g.* polymers or gels). When choosing groups to act as SBUs and give rise to structure extension in the solid-state (through crystal engineering approaches) often moieties rich in hydrogen bond

donors and/or acceptors, π-stacking groups or halogen bonding groups are selected.[25-27] One particularly good SDG that makes use of π-based interactions (π···π stacking, anion···π interactions, C-H···π interactions and solvent···π interactions) is the 1,8-naphthalimide moiety. The electron deficient nature of 1,8-naphthalimide π-systems has been utilised previously to develop metal containing extended networks. Reger and co-workers have pioneered much of this work having elegantly used a variety of metal coordinating sites attached to 1,8-naphthalimides and investigated the extended structures in the solid-state for the development of 3D networks and coordination polymers.[28-36] In addition to crystal engineering, SDGs have also been utilised for immobilisation of functional metal complexes onto surfaces. For example, through the incorporation of hydrophobic functional groups to introduce amphiphilicity, metal complexes can be immobilised into ordered monolayers using Langmuir-Blodgett deposition.[14, 37-40]

Whilst incorporation into the ligand scaffolds of metal complexes is the most common method to introduce SDGs, an alternative approach, and one that has received comparatively little attention, is to incorporate the SDG into the counter ion. Moreover, given the important role that anions play in the structure, packing and sometimes physical properties of coordination complexes, it is somewhat surprising that there has been little synthetic effort focused on developing anions with targeted structure directing properties. Investigating the ability of anions to influence structure and properties of metal complexes opens up access to a vast range of complexes where systems with interesting properties can be further organised into advanced supramolecular materials.

Herein we report the synthesis, characterisation, and structural analysis of four novel 1,8-naphthalimide sulfonate based anions **1** – **4** (Scheme 1) and investigate their ability to alter the

structure of a thiosemicarbazone Fe^{III} coordination complex $[Fe(\mathbf{L_1})_2](\boldsymbol{X})$. We also report an investigation into the use of hexadecylsulfonate (**5**) as a SDG for the immobilisation of $[Fe(\mathbf{L_1})_2](\boldsymbol{X})$ into solid supports using the LB technique. The thiosemicarbazone complex was chosen, as it is a class of solution-stable coordination complex that we are actively investigating in our research group for potentially interesting magnetic properties (*i.e.* Spin-Crossover[41]) as well as developing interesting supramolecular constructs.[42] Organo-sulfonate based systems were utilised in this study as they offer a relatively straightforward synthetic route to organic based designer anions.[43]

EXPERIMENTAL SECTION

General Information. All chemicals were purchased from commercial sources and used as received. Solvents were HPLC grade and were used without further purification. The thiosemicarbazone ligand $\mathbf{L_1}$ was prepared according to our published procedure.[44] Microanalytical data was collected on a Exeter Analytical CE 440 elemental analyzer at University College Dublin. Infrared spectra were recorded on a Thermo Scientific Nicolet iS10 spectrometer with Smart ITR accessory between 400-4000 cm^{-1}. UV-visible spectra were recorded on a Perkin Elmer Lambda 265 spectrophotometer, using either a Single Cell holder or an Advanced Transmission Holder. NMR spectra were recorded on a Bruker DPX400 NMR spectrometer at 300 K. Chemical shifts are reported in parts per million and referenced to the residual solvent peak ($(CD_3)_2SO$: ^1H δ 2.50 ppm, ^{13}C δ 39.52 ppm). Standard conventions indicating multiplicity were used: m = multiplet, t = triplet, d = doublet, s = singlet. Aromatic rings were abbreviated as followed: *Naph* = naphthalimide, *Nap* = naphthalene, *py* = pyridyl, *ph* =

phenyl. Mass spectrometry samples were analysed using a MaXis (Bruker Daltonics, Bremen, Germany) mass spectrometer equipped with a Time of Flight (TOF) analyser. Samples were introduced to the mass spectrometer via a Dionex Ultimate 3000 auto-sampler and uHPLC pump [Gradient 20% acetonitrile (0.2% formic acid) to 100% acetonitrile (0.2% formic acid) in five minutes at 0.6 mL min. Column: Acquity UPLC BEH C18 (Waters) 1.7 micron 50 x 2.1mm]. High-resolution mass spectra were recorded using positive/negative ion electrospray ionization. Fluorescence measurements were carried out using an Agilent Technologies Cary Eclipse fluorescence spectrophotometer. Single-crystal X-ray diffraction data was collected at 100 K on either a Rigaku AFC12 goniometer equipped with an enhanced sensitivity (HG) Saturn 724+ detector mounted at the window of an FR-E+ Superbright Mo-K_α rotating anode generator (λ = 0.71075 Å) with HF or VHF varimax optics, or a Rigaku 007 HF diffractometer equipped with an enhanced sensitivity Saturn 944+ detector with a Cu-Kα rotating anode generator (λ = 1.5418 Å) with HF varimax optics.[45] Unit cell parameters were refined against all data and an empirical absorption correction applied in either CrystalClear[46] or CrysalisPro.[47] All structures were solved by direct methods using SHELXS-2013[48] and refined on F_O^2 by SHELXL-2013[48] using Olex2.[49] H-atoms were positioned geometrically and refined using a riding model. All non-H atoms were refined as anisotropic except for the minor component of the disordered naphthalene in [Fe($\mathbf{L_1}$)$_2$]($\mathbf{3}$)·2½H_2O and the minor component of the disordered naphthalimide in {[Fe($\mathbf{L_1}$)$_2$]($\mathbf{4}$)}$_2$·H_2O·MeOH which were left as isotropic. The solvent masking routine in Olex2 was used in the structures of $\mathbf{4}$·py and {[Fe($\mathbf{L_1}$)$_2$]($\mathbf{4}$)}$_2$·H_2O·MeOH to mask the disordered electron density that corresponded to approximately one and three diethylether molecules respectively. CCDC entries 1527317-1527324 and 1567225 contain the crystallographic data for the structures reported in this article. Langmuir studies: pressure–area isotherms and time stability were

measured at 25 °C on a Kibron MicroTroughXS (MTXS) Langmuir-Blodgett trough. Water for the sub-phase was purified with a Milli-Q® Integral system (Millipore), and its resistivity was measured to be higher than 18 MΩ cm. Chloroform (HPLC grade, Fisher) was used as spreading solvent for [Fe($\mathbf{L_1}$)$_2$](**5**). Typically, drops (20 μl) of the surfactant solution (~0.5 mgmL^{-1}) were deposited using a microsyringe onto the sub-phase. After leaving the solvent to evaporate for ~20 min, the barriers were compressed at 7 mm min^{-1} and the surface pressure was monitored using a platinum DyneProbe that had been flamed. The quartz substrate for Langmuir-Blodgett deposition was made hydrophobic as per the procedure given by Marheineke *et al*., except dichlorodimethylsilane was used instead of trimethoxy(7-octen-1-yl)silane.[50]

General procedure for the synthesis of pyridinium N-(R-SO$_3$)-1,8-naphthalimides ***1 – 4***.

To a stirred suspension of 1,8-naphthalic anhydride (3.00 g, 15 mmol) in pyridine (15 mL) the appropriate amine (15 mmol) was added and the reaction was refluxed for 8 hours. The solution was cooled to room temperature and the resulting solid was filtered and washed thoroughly with diethyl ether (30 mL) to remove residual pyridine.

Pyridinium N-(p-aminobenzenesulfonate)-1,8-naphthalimide (**1**) ·PyH.

The precipitate was an off white powder (4.59 g, 72%). Anal. Calcd for $C_{23}H_{16}N_2O_5S\cdot\frac{1}{3}H_2O$: C, 63.01; H, 3.83; N, 6.39. Found: C, 63.26; H, 3.55; N, 6.19. HRMS (ESI-): Calculated for (**1**)$^-$ *m/z* = 352.0285, found m/z = 352.0279. FTIR (ATR, cm^{-1}): 3211, 3066, 1697, 1654,1586, 1488, 1347, 1355, 1216, 1180; UV/vis (λ_{max}, MeOH): 333 nm, ε = 13,900 L mol^{-1} cm^{-1}; ^{1}H NMR (400 MHz, DMSO-d_6, ppm): δ = 8.96 (dd, J = 6.7, 1.5 Hz, 2H, *Py-H*), 8.65-8.60 (m, 1H, *Py-H*), 8.48 (d, J = 8.0 Hz, 2H, *Naph-H*), 8.47 (d, J = 7.4 Hz, 2H, *Naph-H*), 8.10 (dd, J = 7.8, 6.7 Hz, 2H, *Py-H*), 7.87 (dd, *J* = 8.0, 7.5 Hz, 2H, *Naph-H*), 7.80 (d, J = 8.5 Hz, 2H, *Ph-H*), 7.38 (d, J = 8.5 Hz, 2H, *Ph-H*).

^{13}C NMR (101 MHz, DMSO-d_6, ppm): δ = 163.7, 147.9, 146.6, 142.1, 136.3, 134.6, 131.4, 130.8, 128.6, 127.8, 127.4, 127.2, 126.3, 122.5. Single crystals of **1**·Me_2NH_2 were obtained as large light orange blocks by slow evaporation of DMF (after heating at 130°C for 12 hours). Crystal Data for $C_{20}H_{18}N_2O_5S$ (M =398.42 g/mol): triclinic, space group P-1 (no. 2), a = 8.27110(15) Å, b = 8.56996(16) Å, c = 13.9226(3) Å, α = 77.2422(17)°, β = 85.3921(16)°, γ = 66.6708(18)°, V = 883.80(3) Å^3, Z = 2, T = 100 K, μ(MoKα) = 0.221 mm^{-1}, *Dcalc* = 1.497 g/cm^3, 16000 reflections measured (5.29° ≤ 2θ ≤ 49.992°), 3106 unique (R_{int} = 0.0167, R_{sigma} = 0.0077) which were used in all calculations. The final R_1 was 0.0311 (I > 2σ(I)) and wR_2 was 0.0814 (all data).

Pyridinium N-(m-aminobenzenesulfonate)-1,8-naphthalimide (**2**)·PyH.

The precipitate was an off white powder (3.34 g, 52%). Anal. Calcd for $C_{23}H_{16}N_2O_5S·⅓H_2O$: C, 63.01; H, 3.83; N, 6.39. Found: C, 62.91; H, 3.58; N, 6.20. HRMS (ESI-): Calculated for (**1**)$^-$ *m/z* = 352.0285, found m/z = 352.0277. FTIR (ATR, cm^{-1}): 3072, 1699, 1660, 1584, 1489, 1435, 1355, 1234, 1170, 1029, 996; UV/vis (λ_{max}, MeOH): 333 nm, ε = 16,700 L mol^{-1} cm^{-1}; ^{1}H NMR (400 MHz, DMSO-d_6, ppm): δ = 8.95 (dd, J = 6.6, 1.5 Hz, 2H, *Py-H*), 8.60-8.64 (m, 1H, *Py-H*), 8.48 (d, J = 8.2 Hz, 2H, *Naph-H*), 8.47 (d, J = 7.4 Hz, 2H, *Naph-H*), 8.09 (dd, J = 7.8, 6.6 Hz, 2H, *Py-H*), 7.87 (dd, *J* = 8.5, 7.7 Hz, 2H, *Naph-H*), 7.76-7.73 (m, 1H, *Ph-H*), 7.69-7.68 (m, 1H, *Ph-H*), 7.52 (dd, *J* = 7.8 Hz, 1H, *Ph-H*), 7.39-7.36 (m, 1H, *Ph-H*). ^{13}C NMR (101 MHz, DMSO-d_6, ppm): δ = 163.7, 148.9, 146.6, 142.1, 135.5, 134.5, 131.4, 130.7, 129.5, 128.5, 127.8, 127.3, 127.2, 126.4, 125.5, 122.6. Single crystals of **2**·Me_2NH_2 were obtained as large colorless needles by slow evaporation of DMF (after heating at 130°C for 12 hours). Crystal Data for $C_{20}H_{18}N_2O_5S$ (M =398.42 g/mol): triclinic, space group P-1 (no. 2), a = 8.1427(4) Å, b = 8.5440(3) Å, c = 14.7488(8) Å, α = 86.266(4)°, β = 81.629(4)°, γ = 62.326(5)°, V = 899.03(8) Å^3, Z = 2, T =

100 K, μ(MoKα) = 0.217 mm^{-1},*Dcalc* = 1.472 g/cm^3, 3753 reflections measured (5.584° ≤ 2θ ≤ 49.976°), 2858 unique (R_{int} = 0.0145, R_{sigma} = 0.0248) which were used in all calculations. The final R_1 was 0.0341 (I > 2σ(I)) and wR_2 was 0.0912 (all data).

Pyridinium N-(5-amino-1-naphthalenesulfonate)-1,8-naphthalimide (**3**)·PyH.

The precipitate was a very pale purple powder (5.54 g, 77%). Anal. Calcd for $C_{27}H_{18}N_2O_5S·1½H_2O$: C, 63.65; H, 4.15; N, 5.58. Found: C, 63.21; H, 3.79; N, 5.50. HRMS (ESI-): Calculated for $(\mathbf{3})^-$ *m/z* = 402.0442, found m/z = 402.0441. FTIR (ATR, cm^{-1}): 3069, 2688, 2132, 1705, 1667, 1622, 1586, 1488, 1375, 1350, 1238, 1153; UV/vis (λ_{max}, MeOH): 332 nm, ε = 15,600 L mol^{-1} cm^{-1}; ^{1}H NMR (400 MHz, DMSO-d_6, ppm): δ = 9.06 (d, *J* = 8.2 Hz, 1H, *Nap-H*), 8.93 (dd, *J* = 6.5, 1.5 Hz, 2H, *Py-H*), 8.59-8.53 (m, 5H, *4Naph-H 1Py-H)*, 8.05 – 8.02 (m, *3*H, *2Py-H* 1*Nap-H)*, 7.93 (dd, *J* = 7.8 Hz, 2H, *Naph-H*), 7.80 (d, *J* = 8.3, Hz, 1H, *Nap-H*), 7.70 – 7.62 (m, 2H, *Nap-H*), 7.40 (dd, *J* = 8.7, 7.5 Hz, 1H, *Nap-H*). ^{13}C NMR (101 MHz, DMSO-d_6, ppm): δ = 164.0, 146.0, 144.4, 142.4, 134.7, 132.8, 131.6, 130.9, 130.7, 129.9, 128.5, 128.2, 127.3, 127.1, 126.7, 125.5, 125.4, 124.7, 124.0, 122.6. Single crystals of (**3**)·PyH were obtained as large pale purple needles by recrystallization from toluene. Crystal Data for $C_{27}H_{18}N_2O_5S$ (*M* =482.49 g/mol): monoclinic, space group *Pc* (no. 7), *a* = 7.2420(2) Å, *b* = 20.0409(5) Å, *c* = 7.6589(2) Å, β = 100.378(3)°, *V* = 1093.40(5) $Å^3$, *Z* = 2, *T* = 100 K, μ(CuKα) = 1.697 mm^{-1}, *Dcalc* = 1.466 g/cm^3, 4501 reflections measured (4.41° ≤ 2θ ≤ 129.924°), 2366 unique (R_{int} = 0.0341, R_{sigma} = 0.0370) which were used in all calculations. The final R_1 was 0.0384 (I > 2σ(I)) and wR_2 was 0.1007 (all data).

Pyridinium N-(5-amino-2-naphthalenesulfonate)-1,8-naphthalimide (**4**)·PyH.

The precipitate was an off-white powder (5.91 g, 81%). Anal. Calcd for $C_{27}H_{18}N_2O_5S \cdot \frac{1}{3}H_2O$: C, 66.38; H, 3.85; N, 5.73. Found: C, 66.19; H, 3.60; N, 5.66. HRMS (ESI-): Calculated for $(\mathbf{4})^-$ *m/z* = 402.0442, found m/z = 402.0451. FTIR (ATR, cm^{-1}): 3063, 2603, 1702, 1661, 1583, 1482, 1370, 1345, 1226, 1150; UV/vis (λ_{max}, MeOH): 332 nm, ε = 16,000 L mol^{-1} cm^{-1}; ^{1}H NMR (400 MHz, DMSO-d_6, ppm): δ = 8.84 (dd, J = 6.4, 1.5 Hz, 2H, *Py-H*), 8.57 – 8.53 (m, 4H, *Naph*-H), 8.41-8.37 (m, 1H, *py-H*), 8.31 (d, *J* = 1.2 Hz, 1H, *Nap-H*), 8.15 (d, *J* = 7.7 Hz, 1H, *Nap-H*), 7.94 (dd, J = 8.0, 7.4 Hz, 2H, *Naph-H*), 7.91-7.88 (m, 2H, *Py-H*), 7.77 (d, *J* = 8.8, 1H, *Nap-H*), 7.70 – 7.64 (m, 3H, *Nap-H*). ^{13}C NMR (101 MHz, DMSO-d_6, ppm): δ = 163.9, 145.9, 144.1, 143.7, 134.7, 133.1, 132.8, 131.6, 130.9, 129.9, 129.4, 128.2, 127.6, 127.3, 126.4, 126.2, 124.9, 124.4, 122.6, 122.4. Single crystals of (**4**)·PyH were obtained as large colorless needles by vapor diffusion of diethylether into methanol. Crystal Data for $C_{27}H_{18}N_2O_5S$ (M =482.49 g/mol): triclinic, space group *P*-1 (no. 2), a = 9.43726(18) Å, b = 11.11578(19) Å, c = 11.7097(2) Å, α = 96.4085(15)°, β = 100.5493(16)°, γ = 93.5152(14)°, V = 1195.86(4) Å^3, Z = 2, T = 100 K, μ(MoKα) = 0.177 mm^{-1}, *Dcalc* = 1.340 g/cm^3, 23579 reflections measured (4.406° ≤ 2θ ≤ 60.748°), 6620 unique (R_{int} = 0.0165, R_{sigma} = 0.0132) which were used in all calculations. The final R_1 was 0.0448 (I > 2σ(I)) and wR_2 was 0.1359 (all data).

*General procedure for the synthesis of [Fe(**L**$_1$)$_2$](**X**) where X = **1** – **4**.*

To a heated (50 °C) and stirred pale yellow solution of $\mathbf{L_1}$ (28 mg, 0.1 mmol) in methanol (10 mL) was added $Fe(NO_3)_3 \cdot 9H_2O$ (20 mg, 0.05 mmol, in 5mL methanol) resulting in a very dark yellow/brown solution. Immediately, a solution of the 1,8-naphthalimides (**1** – **4**·PyH, 0.05 mmol) in methanol (9 mL) and DMF (1 mL) was added and the dark solution heated with stirring

at 60°C for 30 minutes. The resulting reaction solution was cooled to room temperature and subjected to vapor diffusion of diethyl ether or slow evaporation.

*[Fe($\mathbf{L_1}$)$_2$](**1**):* Slow evaporation yielded large very dark orange crystals (14 mg, 29%) that were easily physically separated from long colorless needles. Anal. Calcd for $C_{42}H_{32}N_9O_5S_5Fe{\cdot}3H_2O$: C, 49.80; H, 3.78; N, 12.44. Found: C, 49.46; H, 3.39; N, 12.42. HRMS (ESI+): Calculated for $[Fe(\mathbf{L_1})_2]^+$ *m/z* = 606.0194, found *m/z* = 606.0191. HRMS (ESI-): Calculated for [**1**]$^-$ *m/z* = 352.0285, found m/z = 352.0283. FTIR (ATR, cm^{-1}): 3567, 3257, 3059, 1699, 1660, 1499, 1433, 1373, 1171, 1136. UV/vis (λ_{max}, MeOH): 394 nm (ε = ~36,000 L mol^{-1} cm^{-1}). Crystal Data for $C_{42}H_{36}FeN_9O_7S_5$ (*M* =994.95 g/mol): monoclinic, space group $P2_1/n$ (no. 14), *a* = 10.3970(4) Å, *b* = 38.6830(16) Å, *c* = 11.0305(4) Å, β = 105.379(4)°, *V* = 4277.5(3) Å^3, *Z* = 4, *T* = 100 K, μ(MoKα) = 0.660 mm^{-1}, *Dcalc* = 1.545 g/cm^3, 31369 reflections measured (4.212° ≤ 2θ ≤ 49.998°), 7539 unique (R_{int} = 0.0522, R_{sigma} = 0.0499) which were used in all calculations. The final R_1 was 0.0688 (I > 2σ(I)) and wR_2 was 0.1336 (all data).

*[Fe($\mathbf{L_1}$)$_2$](**2**):* Slow evaporation yielded large very dark orange crystals (15 mg, 31%) that were easily physically separated from long colorless needles. Anal. Calcd for $C_{42}H_{32}N_9O_5S_5Fe{\cdot}2½H_2O$: C, 50.25; H, 3.71; N, 12.56. Found: C, 49.98; H, 3.49; N, 12.71. HRMS (ESI+): Calculated for $[Fe(\mathbf{L_1})_2]^+$ *m/z* = 606.0194, found *m/z* = 606.0203. HRMS (ESI-): Calculated for [**2**]$^-$ *m/z* = 352.0285, found m/z = 352.0288. FTIR (ATR, cm^{-1}): 3023, 3087, 1701, 1662, 1505, 1565, 1439, 1374, 1305, 1238, 1184, 1150. UV/vis (λ_{max}, MeOH): 398 nm (ε = ~35,500 L mol^{-1} cm^{-1}). Crystal Data for $C_{44}H_{40}FeN_9O_7S_5$ (*M* =1023.00 g/mol): monoclinic, space group $P2_1/c$ (no. 14), *a* = 10.8378(7) Å, *b* = 27.3619(12) Å, *c* = 15.6774(8) Å, β = 101.214(5)°, *V* = 4560.3(4) Å^3, *Z* = 4, *T* = 100 K, μ(MoKα) = 0.621 mm^{-1}, *Dcalc* = 1.490 g/cm^3, 21529 reflections measured (3.832° ≤

$2\theta \leq 49.994°$), 8040 unique (R_{int} = 0.0560, R_{sigma} = 0.0725) which were used in all calculations. The final R_1 was 0.0656 ($I > 2\sigma(I)$) and wR_2 was 0.1577 (all data).

*[Fe(**L**$_1$)$_2$](**3**):* Vapor diffusion of diethyl ether into the reaction solution yielded very dark orange/red crystals (21 mg, 41%). Anal. Calcd for $C_{46}H_{34}N_9O_5S_5Fe{\cdot}3H_2O$: C, 51.97; H, 3.79; N, 11.86. Found: C, 52.33; H, 3.48; N, 11.34. HRMS (ESI+): Calculated for $[Fe(\mathbf{L_1})_2]^+$ *m/z* = 606.0194, found *m/z* = 606.0204. HRMS (ESI-): Calculated for [**3**]$^-$ *m/z* = 402.0442, found m/z = 402.0447. FTIR (ATR, cm^{-1}): 3257, 3076, 1701, 1657, 1497, 1433, 1373, 1181, 1148, 1052, 1019. UV/vis (λ_{max}, MeOH): 398 nm (ε = ~32,000 L mol^{-1} cm^{-1}). Crystal Data for $C_{46}H_{39}FeN_9O_{7.5}S_5$ (*M* =1054.01 g/mol): monoclinic, space group $P2_1/n$ (no. 14), a = 9.6101(5) Å, b = 40.4746(12) Å, c = 12.7566(4) Å, β = 95.419(3)°, V = 4939.7(3) Å^3, Z = 4, T = 100 K, μ(CuKα) = 4.927 mm^{-1}, *Dcalc* = 1.417 g/cm^3, 40470 reflections measured ($7.296° \leq 2\theta \leq 129.996°$), 8390 unique ($R_{int}$ = 0.0622, R_{sigma} = 0.0371) which were used in all calculations. The final R_1 was 0.1086 ($I > 2\sigma(I)$) and wR_2 was 0.3154 (all data).

*[Fe(**L**$_1$)$_2$](**4**):* Vapor diffusion of diethyl ether into the reaction solution yielded very dark orange/red crystals (30%). Anal. Calcd for $C_{46}H_{34}N_9O_5S_5Fe$: C, 54.76; H, 3.40; N, 12.49. Found: C, 54.26; H, 3.36; N, 12.24. HRMS (ESI+): Calculated for $[Fe(\mathbf{L_1})_2]^+$ *m/z* = 606.0194, found *m/z* = 606.0201. HRMS (ESI-): Calculated for [**4**]$^-$ *m/z* = 402.0442, found m/z = 402.0447. FTIR (ATR, cm^{-1}): 3060, 2810, 1680, 1660, 1570, 1430, 1370, 1230, 1170, 1150, 1020. UV/vis (λ_{max}, MeOH): 348 nm (ε = ~38,000 L mol^{-1} cm^{-1}). Crystal Data for $C_{46.5}H_{37}FeN_9O_6S_5$ (*M* =1034.00 g/mol): triclinic, space group *P*-1 (no. 2), a = 10.3898(3) Å, b = 21.5665(6) Å, c = 22.6561(6) Å, α = 92.346(2)°, β = 96.557(2)°, γ = 91.164(2)°, V = 5037.6(2) Å^3, Z = 4, T =

100 K, μ(MoKα) = 0.562 mm^{-1}, *Dcalc* = 1.363 g/cm^3, 79415 reflections measured (3.622° ≤ 2θ ≤ 52°), 19782 unique (R_{int} = 0.0705, R_{sigma} = 0.0636) which were used in all calculations. The final R_1 was 0.0864 (I > 2σ(I)) and wR_2 was 0.2352 (all data).

*Synthesis of [Fe($\mathbf{L_1}$)$_2$](**5**):*

To a heated (100 °C) and stirred white suspension of sodium hexadecylsulfonate (340 mg, 1.0 mmol) in water (40 mL) an aqueous solution (5 mL) of $Fe(NO_3)_3 \cdot 9H_2O$ (140 mg, 0.35 mmol) was added. The suspension was heated with stirring at 100 °C overnight before being allowed to cool, filtered, and dried. A pale yellow powder was collected of iron(III) tris(hexadecylsulfonate) (216 mg, 0.17 mmol) with a yield of 49%. This iron salt was used without further purification.

To a stirred solution of iron tris(hexadecylsulfonate) (55 mg, 43.1 x10^{-3} mmol) in 3 mL of methanol at room temperature was added solid $\mathbf{L_1}$ (36 mg, 130 x10^{-3} mmol). The resulting dark yellow solution was stirred with heating for 2 h before it was cooled to room temperature and subjected to diffusion of diethyl ether. A dark red/brown microcrystalline solid of *[Fe($\mathbf{L_1}$)$_2$](**5**)* (10.4 mg, 11.4 x10^{-3} mmol) was collected with a yield of 18%. HRMS (ESI+): Anal. Calcd for $C_{40}H_{55}N_8O_3S_5Fe \cdot H_2O$: C, 51.66; H, 6.18; N, 12.05. Found: C, 51.66; H, 6.14; N, 11.75. Calculated for $[Fe(\mathbf{L_1})_2]^+$ *m/z* = 606.0194, found *m/z* = 606.0209. HRMS (ESI-): Calculated for [**5**]$^-$ *m/z* = 305.2156, found m/z = 305.2151. FTIR (ATR, cm^{-1}): 3062, 2915, 2847, 1599, 1498, 1465, 1372, 1184, 1153, 1126, 1031. UV/vis (λ_{max}, MeOH): 398 nm (ε = ~19,500 L mol^{-1} cm^{-1}). Crystal Data for $C_{72}H_{127}FeN_8O_7S_5$ (*M* =1432.96 g/mol): triclinic, space group *P*-1 (no. 2), *a* = 10.8333(5) Å, *b* = 14.5206(8) Å, *c* = 26.7742(14) Å, α = 85.589(4)°, β = 83.128(4)°, γ = 70.282(5)°, *V* = 3933.3(3) $Å^3$, *Z* = 2, *T* = 100 K, μ(MoKα) = 0.378 mm^{-1}, *Dcalc* = 1.210 g/cm^3,

32081 reflections measured (3.3° ≤ 2θ ≤ 49.998°), 13852 unique (R_{int} = 0.0643, R_{sigma} = 0.1131) which were used in all calculations. The final R_1 was 0.1139 (I > 2σ(I)) and wR_2 was 0.3521 (all data).

RESULTS AND DISCUSSION

Synthesis and characterization of naphthalimide anions. 1,8-Naphthalimide anions **1**-**4** were synthesised by the same general procedure (Scheme 1) using a stoichiometric reaction between 1,8-naphthalic anhydride and the appropriate amine [**1** = *p*- aminobenzenesulfonic acid, **2** = *m*-aminobenzenesulfonic acid, **3** = 5-amino-1-naphthalenesulfonic acid and **4** = 5-amino-2-naphthalenesulfonic acid] in refluxing pyridine.

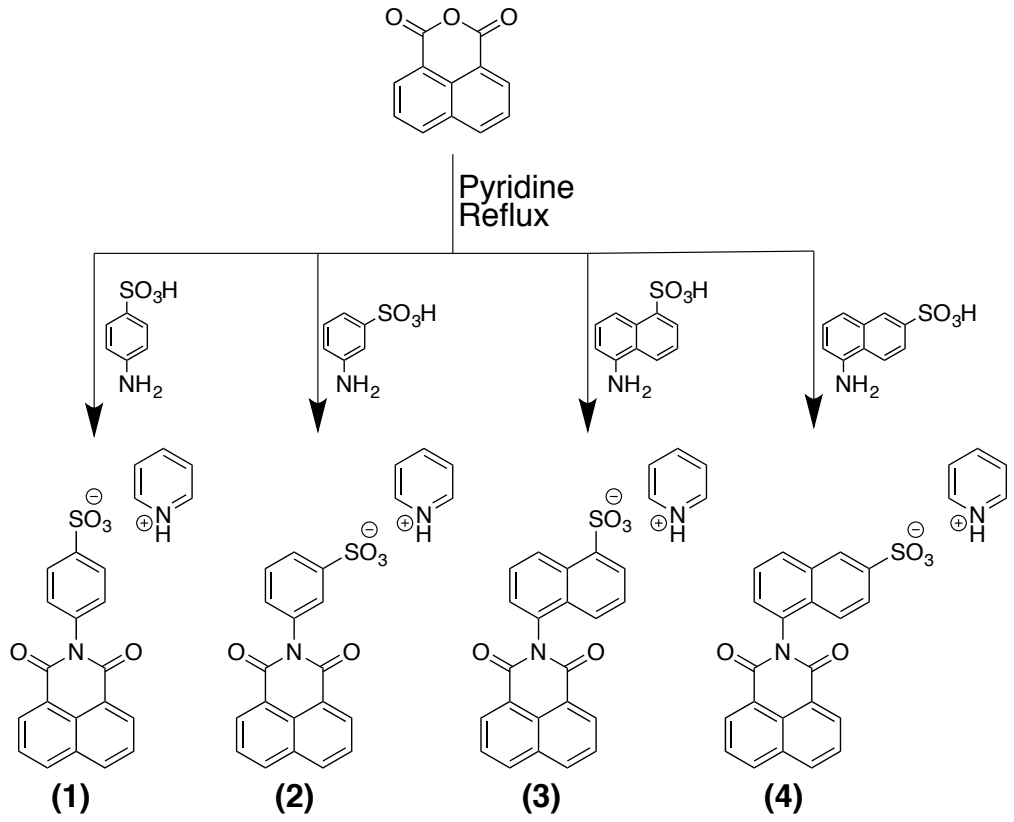

Scheme 1: Synthetic procedure for the synthesis of **1** – **4**·PyH.

On cooling to room temperature followed by filtration, pale colored solids of the pyridinium salts of **1** – **4** were obtained in good yields (~80%). **1** – **4**·PyH were fully characterised using ^{1}H-NMR, ^{13}C-NMR, IR, UV/vis, fluorescence, mass spectrometry and X-ray crystallography (See Supporting Information). All spectroscopic data was consistent with successful formation of the desired compounds. Electronic spectra (absorption and emission) of **1** – **4**·PyH were obtained in MeOH (Fig. S21 and S24). UV/vis spectra of **1**·PyH and **2**·PyH (*ca*. 1x10^{-4} mol L^{-1} in MeOH) displayed nearly identical spectral features with broad absorptions at λ_{max} = 333 nm (ε = 14,000 L mol^{-1} cm^{-1} (**1**) and 16,700 L mol^{-1} cm^{-1} (**2**)) corresponding to transitions originating from the naphthalimide π-system, as observed in similar systems. The emission spectra of **1**·PyH and **2**·PyH displayed broad peaks at ~380 nm (λ_{ex} = 330 nm), both giving stokes shifts of ~ 50 nm. The fluorescence excitation spectra of **1**·PyH and **2**·PyH (λ_{em} = 380 nm) structurally matched those of the corresponding absorption spectra (Fig. S28). The absorption spectra of **3**·PyH and **4**·PyH (*ca*. 1x10^{-4} mol L^{-1} in MeOH) displayed broad absorptions at λ_{max} = 332 nm (ε = 15,600 L mol^{-1} cm^{-1} (**3**) and 16,100 L mol^{-1} cm^{-1} (**4**)) corresponding to transitions originating from the naphthalimide π-system, as observed in **1**·PyH and **2**·PyH. The emission spectra of **3**·PyH and **4**·PyH also displayed broad peaks at ~380 nm (λ_{ex} = 330 nm). The fluorescence excitation spectra of **3**·PyH and **4**·PyH (λ_{em} = 380 nm) structurally matched those of the corresponding absorption spectra (Fig. S29).

Crystallographic characterisation of 1 – 4.

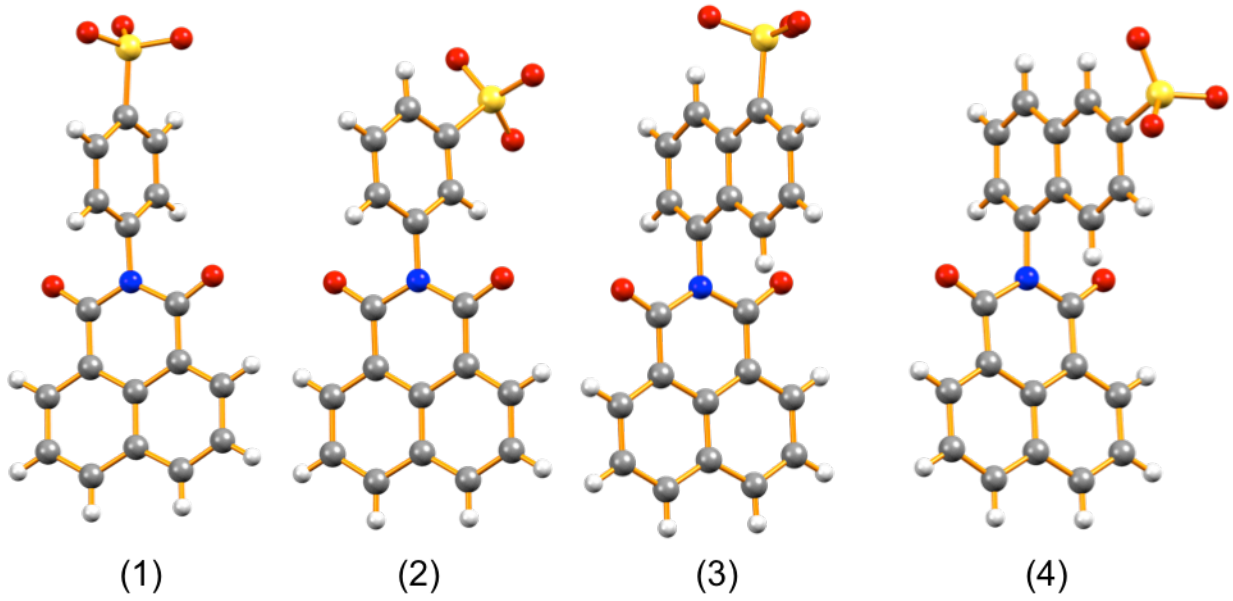

Figure 1: Ball and stick representations of the molecular structures of **1**·NH_2Me_2, **2**·NH_2Me_2, **3**·PyH, and **4**·PyH. Cations omitted for clarity. [Color scheme: S = Yellow; O = Red; N = Blue; C = Grey; H = White.]

Single crystals of **1**·Me_2NH_2 were obtained as large light orange blocks by slow evaporation of DMF (after heating to 130°C) and the low temperature (100 K) molecular structure was obtained. **1**·Me_2NH_2 crystallized in the triclinic space group *P*-1 and contained one molecule in the asymmetric unit (Fig. 1 and S45). The phenyl ring is out of plane with respect to the naphthalimide ring, a feature commonly observed in these ligand systems, with an angle of 74° between the mean planes of the two rings.

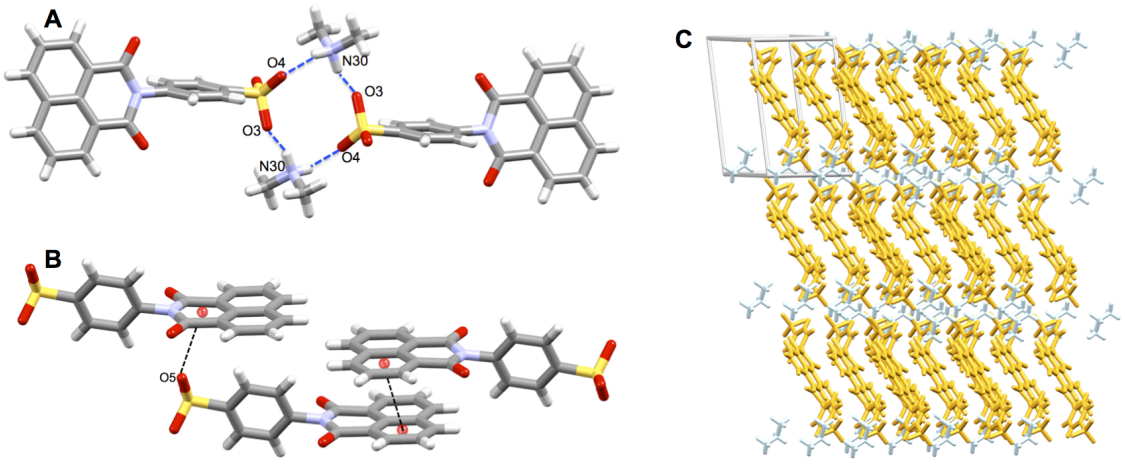

Figure 2: Hydrogen bonding interactions (**A**) and π-based interactions (**B**) present in the solid-state structure of **1**·Me2NH$_2$. Example of the layers formed through interactions (**C**) – *anion shown in orange, cation shown in blue*. H-bonding shown by blue dashed lines: [N30···O3 = 2.718(2) Å and ∠(NH···O) = 160°, and N30···O4 = 2.820(2) Å and ∠(NH···O) = 158°]. π-based interactions shown by black dashed lines: [O5···centroid = 3.308 Å] and [centroid···centroid = 3.534 Å]

The packing interactions in **1**·Me_2NH_2 consist of anion···π interactions, π···π stacking and H-bonding. Naphthalimide molecules are arranged into dimers through H-bonding between two Me_2NH_2 cations and two naphthalimde anions [N30···O3 = 2.718(2) Å and ∠(NH···O) = 160°, and N30···O4 = 2.820(2) Å and ∠(NH···O) = 158°] (Fig. 2). These dimers are then connected to additional dimers through an anion···π interaction between the oxygen atom of the sulfonate (the oxygen atom not involved in the H-bonding) and the imide ring on a neighboring molecule [O5···centroid = 3.308 Å]. Additionally a π···π stacking interaction also exists between the naphthalene moieties on neighbouring molecules [centroid···centroid = 3.534 Å], (Fig. 2). These

interactions ultimately give rise to extended layers of the anion throughout the crystal structure (Fig. 2).

Single crystals of **2**·Me_2NH_2 were obtained as large colorless needles by slow evaporation of DMF (after heating to 130°C) and the low temperature (100 K) molecular structure was obtained. **2**·Me_2NH_2 crystallized in the triclinic space group *P*-1 and contained one molecule in the asymmetric unit (Fig. 1 and S45). As with the previous structure the phenyl ring is oriented out of the naphthalimide plane, with mean plane angles of 66° between the phenyl and imide rings.

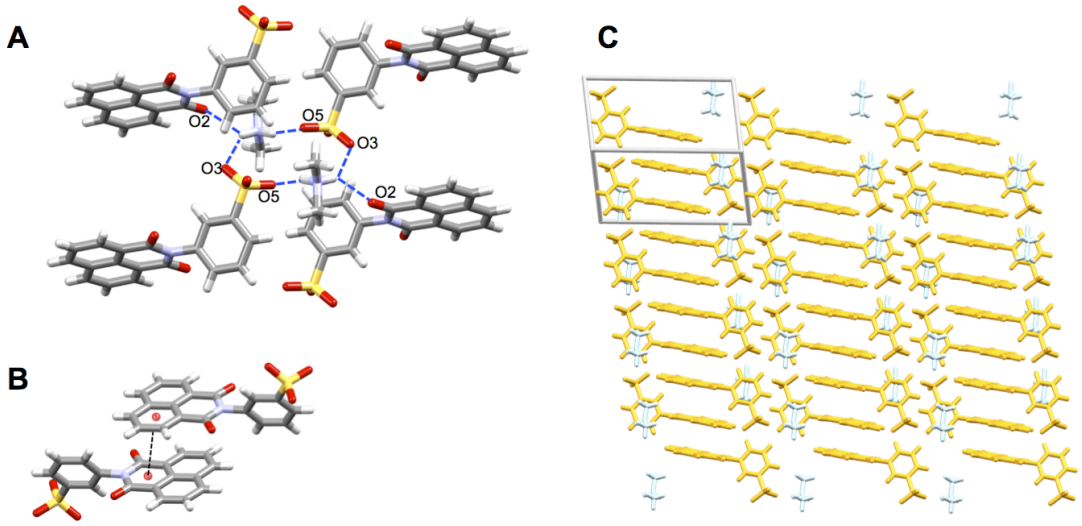

Figure 3: Hydrogen bonding interactions (**A**) and π-based interactions (**B**) present in the solid-state structure of **2**·Me2NH_2. Example of the layers formed through the interactions (**C**) – *anion shown in orange, cation shown in blue*. H-bonding shown by blue dashed lines: [N30···O3 = 2.911(2) Å and ∠(NH···O) = 137°; N30···O5 = 2.795(2) Å and ∠(NH···O) = 162°; and N30···O2 = 3.002(2) Å and ∠(NH···O) = 130°]. π-based interactions shown by black dashed lines: [centroid···centroid = 3.592 Å]

The different position of the sulfonate group gives packing interactions that are significantly different to those observed in **1**·Me_2NH_2. Rather than H-bonding arranging two naphthalimides into a dimer, in **2**·Me_2NH_2 the H-bonding interactions between two Me_2NH_2 cations arrange four naphthalimides into a tetramer *via* strong H-bonding between the NH groups and the oxygen atoms of the sulfonate groups [N30···O3 = 2.911(2) Å and ∠(NH···O) = 137°; N30···O5 = 2.795(2) Å and ∠(NH···O) = 162°]; and weaker H-bonding between the NH groups and the carbonyl oxygen atom of a naphthalimde [N30···O2 = 3.002(2) Å and ∠(NH···O) = 130°] (Fig. 3). These H-bonded tetramers are linked to neighboring assemblies through π···π stacking between neighboring naphthalimide rings [centroid···centroid = 3.592 Å] (Fig. 3). As previously seen these interactions also give rise to extended layers of the anion throughout the crystal structure (Fig. 3).

Single crystals of **3**·PyH were obtained as clear yellow needles by recrystallization from hot toluene and the low temperature (100 K) molecular structure was obtained. **3**·PyH crystallized in the monoclinic space group *Pc* and contained one molecule in the asymmetric unit (Fig. 1 and S45). Similar to the previous structures, the naphthalene group is appoximately orthogonal to the naphthalimide ring with an angle of 82° between the mean planes of the two rings. With the expansion of the phenyl ring to a naphthalene ring, it was expected that π···π stacking would be enhanced, however in this structure no clear π···π stacking to the *naphthalene* ring is observed.

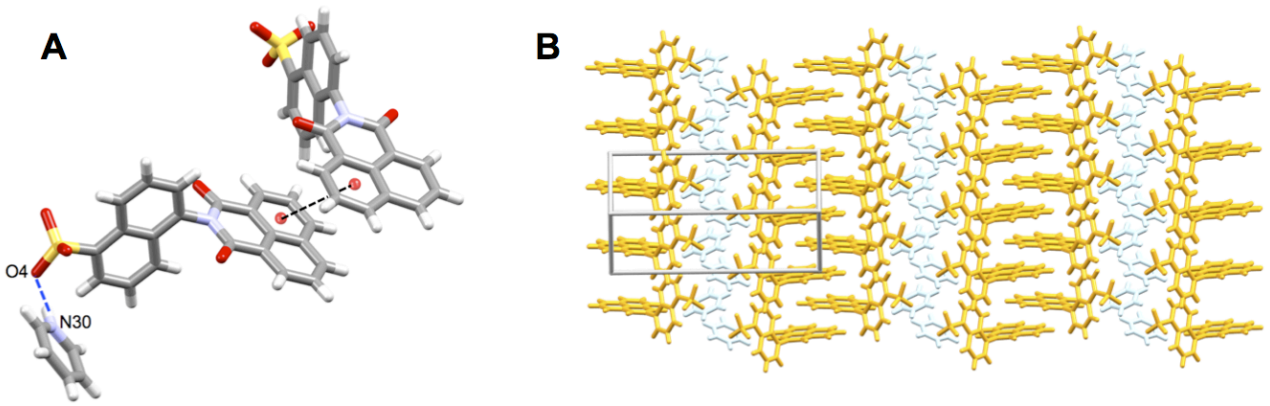

Figure 4: Hydrogen bonding interactions and π-based interactions (**A**) present in the solid-state structure of **3**·PyH. Example of the layers formed by these interactions (**B**) – *anion shown in orange, cation shown in blue*. H-bonding shown by blue dashed line: [N30···O4 = 2.729(5) Å and ∠(NH···O) = 171°].

However, there are weak interactions between neighboring naphthalimide rings – most likely crystal packing effects [centroid···centroid = 3.842 Å] (Fig. 4). These are different to the previous two structures as the π···π stacking gives naphthalimide molecules arranged at approximately 75° to each other (in **1**·Me_2NH_2 and **2**·Me_2NH_2 the naphthalimides are at 180°). There is also a hydrogen bond between the sulfonate group and the pyridinium cation [N30···O4 = 2.729(5) Å and ∠(NH···O) = 171°] however, this interaction appears to have little impact on the overall long range ordering (Fig.4). Despite this compound displaying much weaker intermolecular interactions, the long-range structure is still organized into offset layers (Fig. 4).

Single crystals of **4**·PyH were obtained as clear colorless needles by diffusion of diethyl ether into a methanolic solution of **4**·PyH and the low temperature (100 K) molecular structure was obtained. **4**·PyH crystallized in the monoclinic space group *P*-1 and contained one molecule in the asymmetric unit (Fig. 1 and S45). Interstitial solvent is present within the structure, however a satisfactory disorder model was not found. As such the OLEX[2] Solvent Mask routine was used to

mask the disordered electron density that correlates to approximately one diethyl ether molecule per cell. As with the previous structures the naphthalene group is approximately orthogonal to the naphthalimide ring, with an angle of 84° between the mean planes of the two rings.

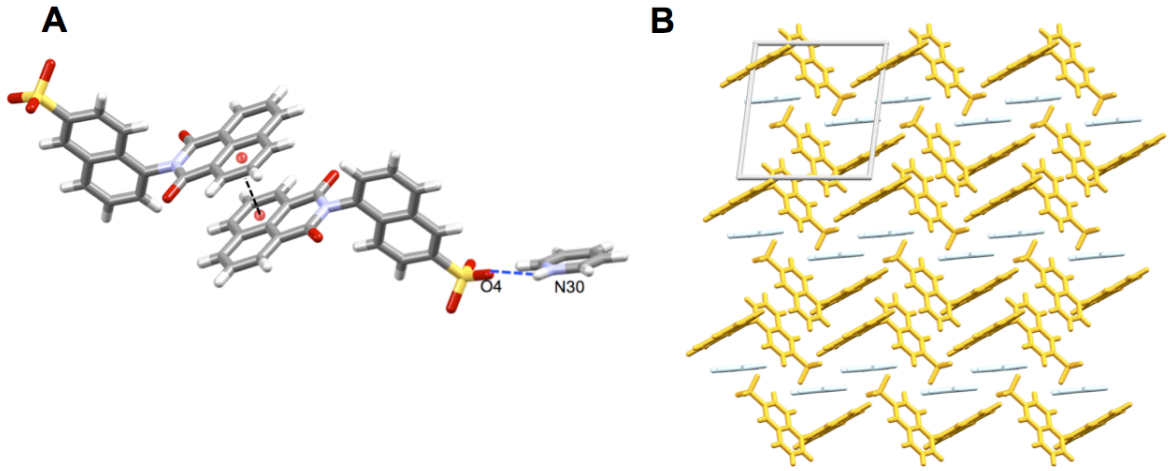

Figure 5: Hydrogen bonding interactions and π-based interactions (**A**) present in the solid-state structure of **4**·PyH. Overall packing arrangement in the solid-state structure of **4**·PyH (**B**) – *anion shown in orange, cation shown in blue*. H-bonding shown by blue dashed line: [N30···O4 = 3.449(2) Å and ∠(NH···O) = 160°]. π-based interactions shown by black dashed line: [centroid···centroid = 3.550 Å].

The solid-state structure shows a π···π stacking interaction between the naphthalimide groups on neighboring molecules [centroid···centroid = 3.550 Å] (Fig. 5), as well as a hydrogen bond between the sulfonate group and the pyridinium cation [N30···O4 = 3.449(2) Å and ∠(NH···O) = 160°] (Fig. 5). As with the three previous compounds, the long-range order present in this structure is formation of layers of the anion (Fig. 5).

Synthesis and characterization of [Fe($\mathbf{L_1}$)$_2$](R-SO$_3$) complexes. Having developed and synthesized the naphthalimide anions, we next investigated introducing organic-sulfonate anions **1** – **5** into the Fe^{III} complex [Fe($\mathbf{L_1}$)$_2$](**X**) in order to explore the structure directing properties of the

anions and how they influenced the overall topology within the complex. In the case of $[Fe(\mathbf{L_1})_2](\mathbf{5})$ we also wanted to investigate whether the introduction of an amphiphilic anion might allow for ordered Langmuir mono-layers to be constructed. Simple one-pot reactions were carried out for the synthesis of $[Fe(\mathbf{L_1})_2](\mathbf{X})$ for X = **1** – **4** where $Fe(NO_3)_3{\cdot}9H_2O$, $\mathbf{L_1}$ and **X** in 1:2:1 ratios were heated at 60°C in MeOH for 30 minutes (Scheme 2).

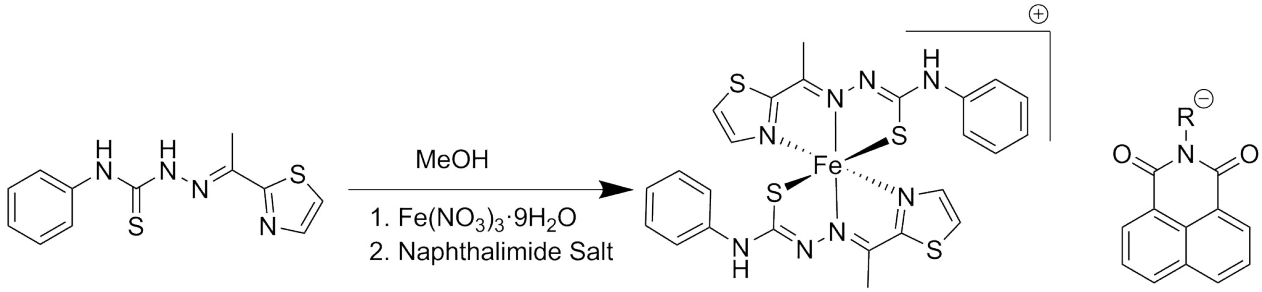

Scheme 2: Synthesis of complexes $[Fe(\mathbf{L_1})_2](\mathbf{X})$ where **X** = **1** – **4** (R = p-aminobenzenesulfonate (**1**), m-aminobenzenesulfonate (**2**), 5-amino-1-naphthalenesulfonate (**3**), 5-amino-2-naphthalenesulfonate (**4**).

The resulting very dark orange/yellow solutions were allowed to cool to room temperature and left to evaporate or subjected to vapor diffusion of diethyl ether resulting in dark orange or red single crystals. When the same one-pot reaction conditions were attempted for $[Fe(\mathbf{L_1})_2](\mathbf{5})$, only $[Fe(\mathbf{L_1})_2](\mathbf{NO_3})$ was isolated. In order to prepare $[Fe(\mathbf{L_1})_2](\mathbf{5})$ an amphiphilic Fe^{III} starting material was first prepared by reaction of $Fe(NO_3)_3{\cdot}9H_2O$ and sodium hexadecylsulfonate in water.

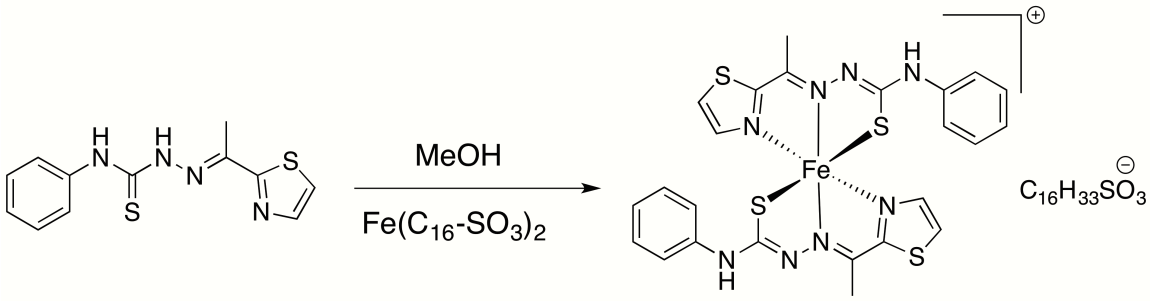

Scheme 3: Synthesis of $[Fe(\mathbf{L_1})_2](\mathbf{5})$.

The resulting solid was filtered, dried and then reacted with $\mathbf{L_1}$ in a 1:3 ratio in MeOH (Scheme 3). The resulting dark yellow solution was stirred at room temperature for 30 minutes before being subjected to vapor diffusion of diethyl ether to afford a dark red/brown crystalline solid. $[Fe(\mathbf{L_1})_2](\mathbf{X})$ for $\mathbf{X} = \mathbf{1} - \mathbf{5}$ were fully characterised using IR, UV-vis, elemental analysis, mass spectrometry and single crystal X-ray crystallography. All data indicated successful formation of the desired compounds and can be found in the supporting information. UV-vis spectra of $[Fe(\mathbf{L_1})_2](\mathbf{1})$ and $[Fe(\mathbf{L_1})_2](\mathbf{2})$ in MeOH (*ca.* $1x10^{-5}$ mol L^{-1}) were dominated by a broad metal based charge transfer band with λ_{max} ~395 nm (ε ~36,000 L mol^{-1} cm^{-1}), in addition to broad features due to the naphthalimide moieties centered at ~340 nm and higher energy transitions at ~250 nm (Fig. S22 and S23). The UV-vis spectra of $[Fe(\mathbf{L_1})_2](\mathbf{3})$ and $[Fe(\mathbf{L_1})_2](\mathbf{4})$ also featured broad features centered at ~340 nm due to the naphthalimide moieties, in addition to broad metal based charge transfer bands at λ_{max} ~390 nm (ε ~35,000 L mol^{-1} cm^{-1}) and higher energy transitions at ~250 nm (Fig. S25 – S26). The UV-vis spectrum of $[Fe(\mathbf{L_1})_2](\mathbf{5})$ (Fig. S27) was similar to the spectra of $[Fe(\mathbf{L_1})_2](\mathbf{1})$ and $[Fe(\mathbf{L_1})_2](\mathbf{2})$ in that it was dominated by a broad metal based charge transfer band λ_{max} ~398 nm (ε ~19,500 L mol^{-1} cm^{-1}) and again higher energy transitions at ~250 nm. IR spectra of all five complexes contained the characteristic peaks associated with SO_3^- groups (*ca.* 1370-1335 cm^{-1} and *ca.* 1195-1165 cm^{-1}). In addition, peaks present in both the spectra of $\mathbf{1} - \mathbf{5}$ and in the corresponding complexes (Fig. S11 - S20) are observed indicating that the bulk samples contain the desired organic sulfonates and not the nitrate anion. High resolution mass spectra collected of the complexes in both positive and negative modes showed ions corresponding to $[Fe(\mathbf{L_1})_2]^+$ (positive mode) and the anions $\mathbf{1} - \mathbf{5}$ (negative mode) (Fig. S34 – S43).

Crystallographic characterisation of [Fe(L_1)$_2$](*R-SO$_3$*) complexes. To fully investigate the structure directing properties of **1** – **5** when included into the structure of potentially functional coordination complexes, single crystals were obtained and the low temperature (100 K) molecular structures determined. Large dark orange block-like single crystals of [Fe($\mathbf{L_1}$)$_2$](**1**)·2H$_2$O were grown by slow evaporation of the reaction solution. [Fe($\mathbf{L_1}$)$_2$](**1**)·2H$_2$O crystallized in the monoclinic space group $P2_1/n$ and contained one complete complex of [Fe($\mathbf{L_1}$)$_2$](**1**) and two interstitial water molecules in the asymmetric unit (Fig. 6). The Fe(III) complex adopts a distorted octahedral geometry, (Σ = 69.5°) [51-53], with an N_4S_2 coordination sphere (Table 1). Packing of the molecule is dominated by H-bonding interactions (Fig. 7).

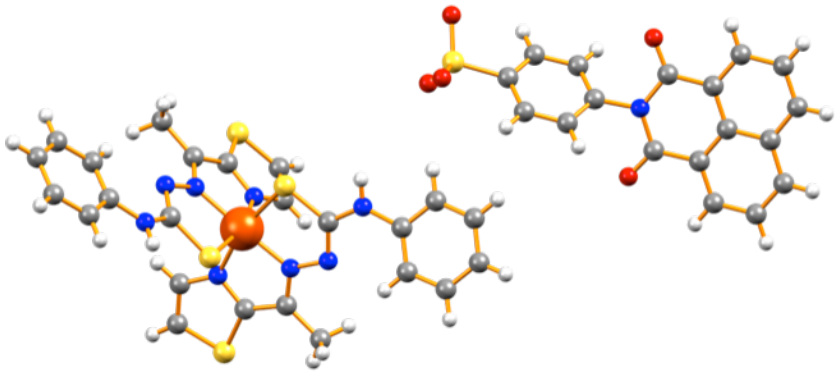

Figure 6: Ball and stick representation of the molecular structure of [Fe($\mathbf{L_1}$)$_2$](**1**)·2H$_2$O. Interstitial water molecules omitted for clarity. [Color scheme: Fe = Orange; S = Yellow; O = Red; N = Blue; C = Grey; H = White.]

The interstitial water molecules play an important role within the packing of this structure, as they form a H-bonding bridge between a thioamine of the complex and the anion. This is achieved through a thioamine NH donor and the oxygen atom of an interstitial water [N21···O100 = 2.830(5) Å and ∠(NH···O) = 165°], and another interaction from the same water to the sulfonate oxygen [O100···O44 = 2.826(5) Å and ∠(OH···O) = 166°] (Fig. 7). This positions the anion in

close proximity to the complex. In addition to this, there is a direct interaction between a thioamine NH donor to a symmetry generated sulfonate group [N1···O44' = 2.925(5) Å and ∠(NH···O)= 165°] showing further interaction between the two components.

Table 1: Selected bond lengths and Σ values in Fe^{III} complexes. General labeling scheme for all complexes is shown.

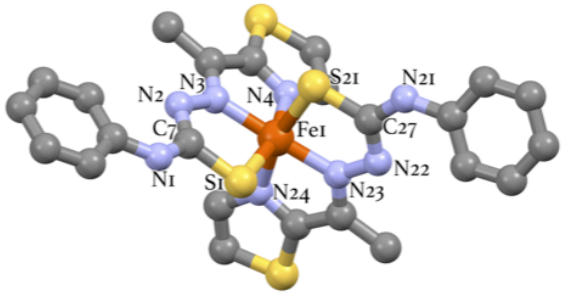

	[Fe(L_1)$_2$](**1**)	[Fe(L_1)$_2$](**2**)	[Fe(L_1)$_2$](**3**)	[Fe(L_1)$_2$](**4**)[a]	[Fe(L_1)$_2$](**5**)
N2 - C7 (Å)	1.310(6)	1.332(6)	1.309(10)	1.298(8)	1.312(9)
S1 - C7 (Å)	1.753(5)	1.760(5)	1.751(8)	1.762(6)	1.755(8)
N22 - C27 (Å)	1.317(6)	1.321(6)	1.302(10)	1.311(7)	1.319(10)
S21 - C27 (Å)	1.747(5)	1.774(5)	1.751(8)	1.752(5)	1.755(7)
Fe1 - S1 (Å)	2.2022(14)	2.2385(15)	2.206(2)	2.2247(17)	2.248(2)
Fe1 - S21 (Å)	2.1996(13)	2.2318(15)	2.221(2)	2.2217(16)	2.217(3)
Fe1 - N4 (Å)	1.976(4)	1.999(4)	1.990(7)	1.985(5)	1.989(6)
Fe1 - N3 (Å)	1.937(4)	1.934(4)	1.931(6)	1.920(5)	1.925(6)
Fe1 - N24 (Å)	1.987(4)	1.987(4)	1.977(7)	1.974(5)	1.972(7)
Fe1 - N23 (Å)	1.933(4)	1.932(4)	1.912(6)	1.926(4)	1.930(6)
Σ (°)	69.5	69.6	76.98	69.2	73.3
Cis angle range (°)	81.0 - 102.9 (15)	80.8-100.4 (17)	78.7 - 104.7 (4)	81.1 - 103.7 (2)	80.7 - 101.8 (18)

[a]*Only the ordered complex molecule is included in the table. Data for the disordered component: N42-C47, 1.316(8); S41-C47, 1.745(8); N62-C67, 1.348(14); S61-C67, 1.800(11); Fe2-S41, 2.2195(18); Fe2-S61, 2.2212(18); Fe2-N44, 1.982(5); Fe2-N43, 1.916(5); Fe2-N63, 1.999(11); Fe2-N64, 2.009(6); Fe2-N67, 1.83(2); Σ (70% component) =77.6°; Cis angle range (70% component) = 77.6 - 103.6 (3); Σ (30% component) =91.5° and Cis angle range (30% component) = 77.0 - 114.2 (8)*

The second water molecule is involved in two interactions, one with a naphthalimide oxygen [O101···O41 = 2.949(6) Å and ∠(OH···O)= 150°], and the other with the first water molecule

[O100···O101 = 2.909(8) Å and ∠(OH···O)= 135°]. Within the complex, the anion structure has deviated significantly from **1**·NH_2Me_2 with the phenyl ring twisted 60° out of plane from the naphthalimide, (compared to 74° observed in **1**·NH_2Me_2). Additionally, unlike the π-based interactions in **1**·NH_2Me_2 the structure of [Fe($\mathbf{L_1}$)$_2$](**1**)·$2H_2O$ does not show naphthalimide···naphthalimide short contacts, instead a naphthalimide···phenyl π-interactions is present [centroid···centroid = 3.570 Å] on one face of the naphthalimide ring, while a much weaker naphthalimide···phenyl crystal packing interaction exists on the opposite face [centroid···centroid = 3.916 Å]. These interactions result in the formation of layers of naphthalimide···phenyl stacks that further arrange the metal cations into columns (Fig. 7).

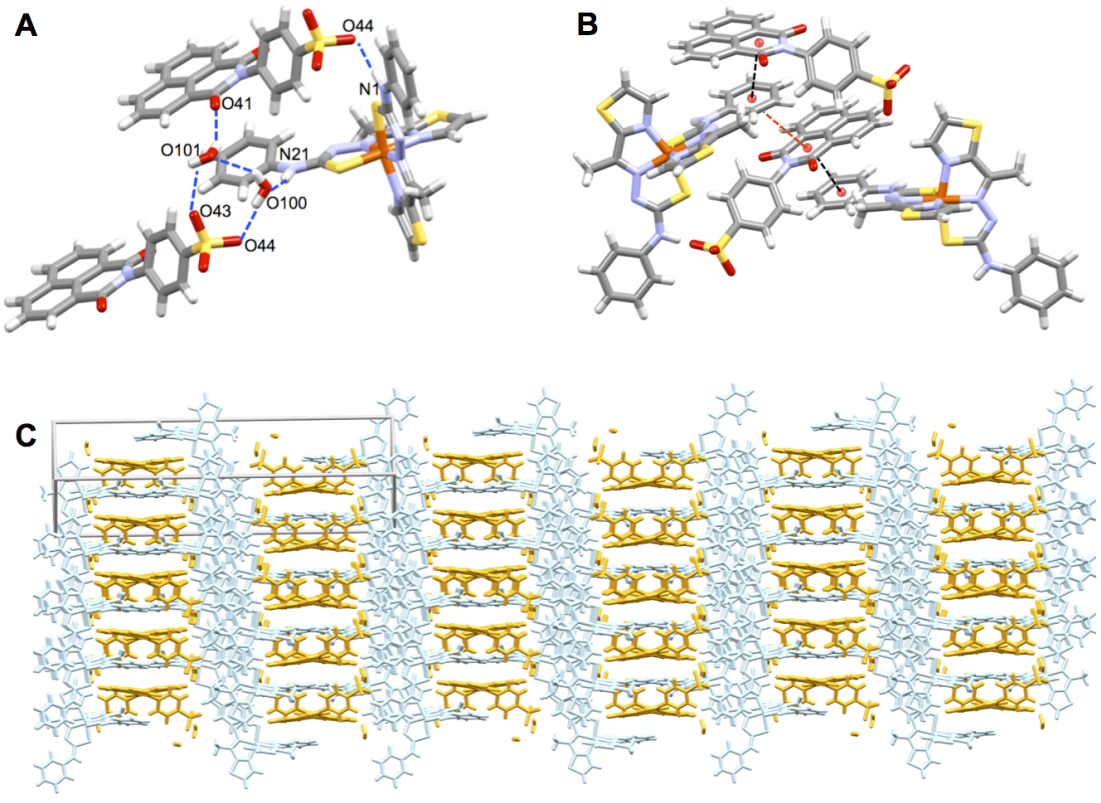

Figure 7: Hydrogen bonding interactions (**A**) and π-based interactions (**B**) present in the solid-state structure of [Fe($\mathbf{L_1}$)$_2$](**1**)·$2H_2O$. Overall packing showing columns of metal complex (in blue) formed through π-interactions to

naphthalimde anion (orange) (**C**). H-bonding shown by blue dashed lines: [N21···O100 = 2.830(5) Å and ∠(NH···O) = 165°; O100···O44 = 2.826(5) Å and ∠(OH···O) = 166°; N1···O44' = 2.925(5) Å and ∠(NH···O)= 165°; O101···O41 = 2.949(6) Å and ∠(OH···O)= 150°; O100···O101 = 2.909(8) Å and ∠(OH···O)= 135°]. Strong π-based interactions shown by black dashed line - [centroid···centroid = 3.570 Å]; weak crystal packing interaction shown by red dashed line [centroid···centroid = 3.916 Å].

Large, dark orange block like crystals of [Fe($\mathbf{L_1}$)$_2$](**2**)·2MeOH were grown by the slow evaporation of the reaction solution. [Fe($\mathbf{L_1}$)$_2$](**2**)·2MeOH crystallized in the monoclinic space group $P2_1/c$ and contained one complete complex of [Fe($\mathbf{L_1}$)$_2$](**2**), and two interstitial methanol molecules (one of which is has the carbon atom disordered over two sites in equal ratios) in the asymmetric unit (Fig. 8). The sulfonate functional group in **2** is also disordered over two sites in equal ratios. Additionally, one of the ligand phenyl rings contains two disordered carbon atoms split over two sites with relative occupancies of 0.6 and 0.4. The structure of the Fe(III) complex is very similar to that observed in the previous structure, *i.e.* similar coordination environment, Σ = 69.6°, and similar bond lengths and angles (Table 1). Packing of the molecule is dominated by hydrogen bonding interactions and, as seen in the previous structure, there is an interaction between the metal complex and the anion bridged by an interstitial solvent molecule (Fig. 9).

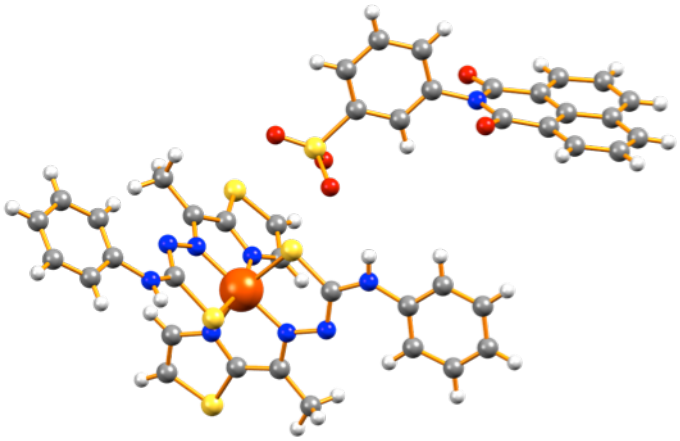

Figure 8: Ball and stick representation of the molecular structure of [Fe($\mathbf{L_1}$)$_2$](**2**)·2MeOH. Interstitial methanol molecules omitted for clarity. [Color scheme: Fe = Orange; S = Yellow; O = Red; N = Blue; C = Grey; H = White.]

This interaction consists of a thioamine to methanol hydrogen bond [N1···O301 = 2.883(6) Å and ∠(NH···O) = 174°] and a hydrogen bond from the same methanol to a symmetry generated sulfonate group [disordered sulfonate component 1: (O301···O103 = 2.574(8) Å and ∠(OH···O) = 177°) and disordered sulfonate component 2: (O301···O106 = 2.967(11) Å and ∠(OH···O) = 164°)]. In addition to this there is an interaction between the other thioamine NH and a naphthalimide carbonyl [N21···O102 = 2.913(5) Å and ∠(NH···O) = 132°]. Finally, the full occupancy interstitial methanol forms a hydrogen bond to the sulfonate group [disordered sulfonate component 1: (O201···O107 = 2.692(11) Å and ∠(OH···O) = 171°) and disordered sulfonate component 2: (O201···O105 = 3.242(14) Å and ∠(OH···O) = 170°)]. The naphthalimide anion in [Fe($\mathbf{L_1}$)$_2$](**2**)·2MeOH is less constrained than in **2**·NH_2Me_2 with the phenyl group twisted out of plane at 88° in the former compared to 66° in the latter. The different position of the sulfonate group in **2** gives rise to significantly different solid-state packing interactions, for example there is no π···π stacking interaction between the metal complex phenyl ring and the

naphthalimide anion (as seen for [Fe($\mathbf{L_1}$)$_2$](**1**)·2H$_2$O) and indeed there is no clear evidence of *any* π···π stacking involving the naphthalimide anions, instead the packing within [Fe($\mathbf{L_1}$)$_2$](**2**)·2MeOH is dominated by hydrogen bonding. This indicates that changing the position of the sulfonate has a dramatic effect on the long range ordering of the complex. Whilst there is no obvious structure directing influence *via* naphthalimide π···π stacking, the overall arrangement of molecules in [Fe($\mathbf{L_1}$)$_2$](**2**)·2MeOH shows ABAB type layers, one of which is the Fe(III) complex, and the other the naphthalimide anions (Fig. 9).

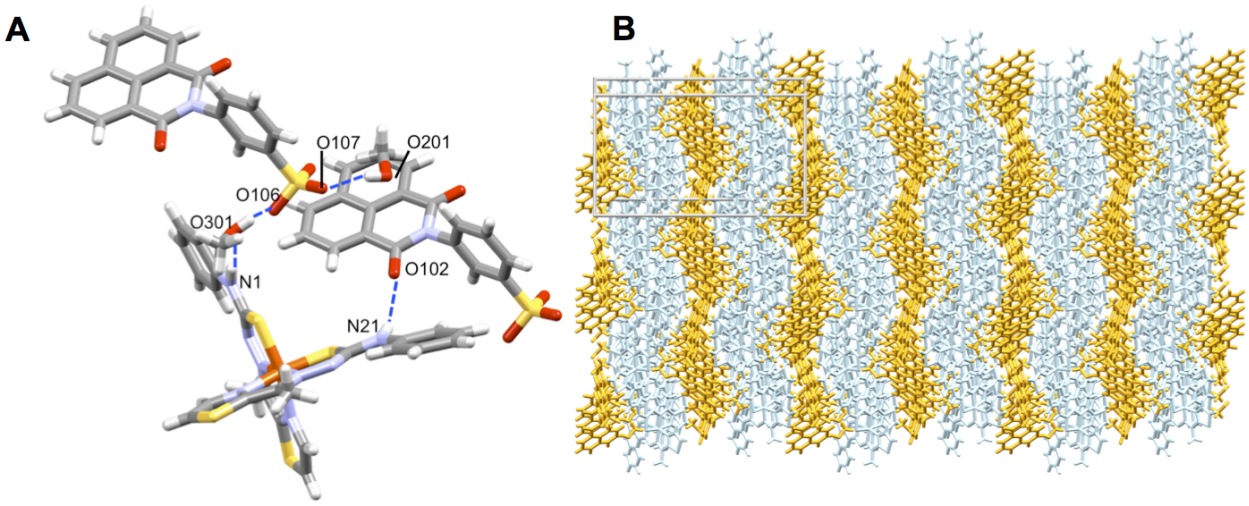

Figure 9: Hydrogen bonding interactions (**A**) present in the solid-state structure of [Fe($\mathbf{L_1}$)$_2$](**2**)·2MeOH. Overall packing showing ABAB layers of metal complex (in blue) and naphthalimde anion (orange) (**B**). H-bonding shown by blue dashed lines: [N1···O301 = 2.883(6) Å and ∠(NH···O) = 174°; O301···O106 = 2.967(11) Å and ∠(OH···O) = 164°; N21···O102 = 2.913(5) Å and ∠(NH···O) = 132°; O201···O107 = 2.692(11) Å and ∠(OH···O) = 171°].

Small dark red block-like crystals of [Fe($\mathbf{L_1}$)$_2$](**3**)·2½H$_2$O were grown by vapour diffusion of diethyl ether into the reaction solution. The complex crystallised in the monoclinic space group $P2_1/n$ and contained one complete molecule of [Fe($\mathbf{L_1}$)$_2$](**3**) and a variety of partial occupancy water molecules totalling 2½ (Fig. 10).

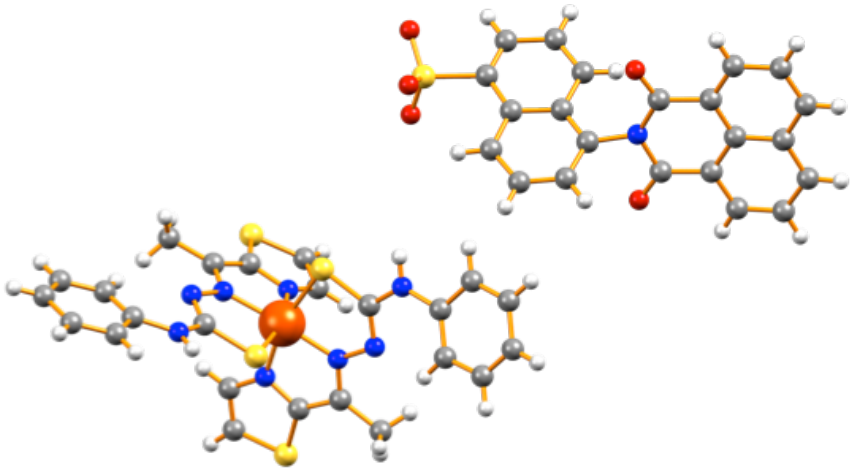

Figure 10: Ball and stick representation of the molecular structure of [Fe($\mathbf{L_1}$)$_2$](**3**)·2½H_2O. Interstitial water molecules and lowest site occupancy disorder omitted for clarity. [Color scheme: Fe = Orange; S = Yellow; O = Red; N = Blue; C = Grey; H = White.]

The Fe(III) complex is similar to the previous two structures in that it is indicative of a LS iron(III) centre with a slightly distorted octahedral geometry, Σ = 76.8°, (N_4S_2 coordination environment). The naphthalimide anion contains a severely disordered nathphthalene-sulfonate component where it is disordered over two sites with relative occupancies of 0.65 and 0.35. Only the packing interactions to the major occupancy component are described. Similar to previous structures, there is an interstitial water molecule that bridges the cation and anion components though H-bonding (Fig. 11) where a thioamine to water hydrogen bond [N21···O100 = 2.824(7) Å and ∠(NH···O) = 157°] and a hydrogen bond from the same water to the sulfonate group of the anion [O100···O44 = 2.671(9) Å] exist. In addition to these two H-bonds there is also an H-bonding interaction between the second thioamine of the complex and a neighboring sulfonate group [N1···O44 = 2.910(7) Å and ∠(NH···O) = 171°] (Fig. 11)

Interestingly in this complex one of the thiosemicarbazone ligands adopts a somewhat bowed structure as a result of a π-stacking interaction to the imide portion of the naphthalimide [centroid···centroid = 3.735 Å] (Fig. 11). The overall packing in [Fe($\mathbf{L_1}$)$_2$](**3**)·2½H_2O is very similar to that observed in [Fe($\mathbf{L_1}$)$_2$](**1**)·2H_2O where columns of cation are separated by naphthalimides. However, the extra bulk of the anion (*i.e*. naphthalene *vs*. phenyl) appears to cause the aforementioned bowing of the thiosemicarbazone and results in a longer centroid···centroid distance (Fig 11).

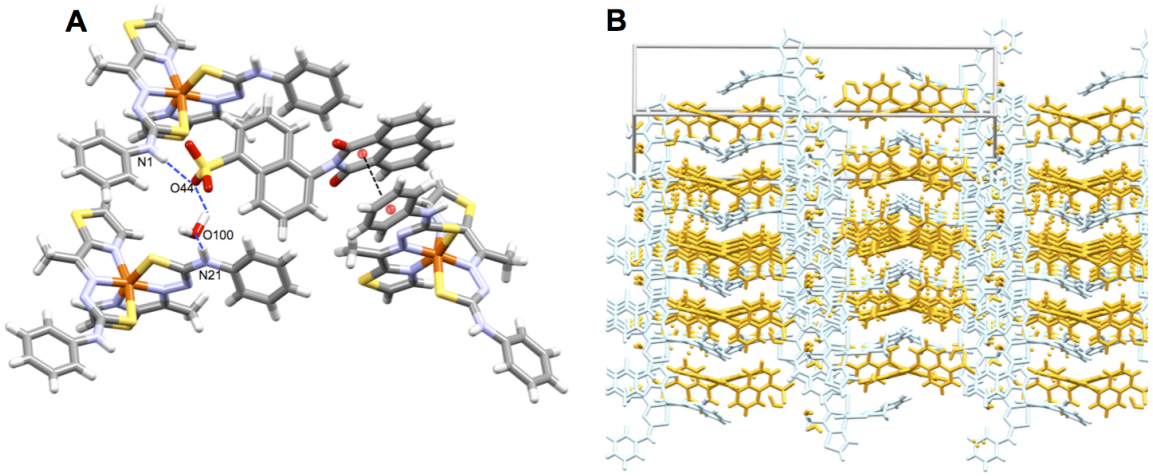

Figure 11: Hydrogen bonding interactions and π-based interactions (**A**) present in the solid-state structure of [Fe($\mathbf{L_1}$)$_2$](**3**)·2½H_2O. Overall packing showing columns of metal complex (in blue) formed through π-interactions to naphthalimde anion (orange) (**B**). H-bonding shown by blue dashed lines: [N21···O100 = 2.824(7) Å and ∠(NH···O) = 157°; O100···O44 = 2.671(9) Å; N1···O44 = 2.910(7) Å and ∠(NH···O) = 171°]. π-based interaction shown by black dashed line - [centroid···centroid = 3.735 Å].

Poor quality dark orange plate-like crystals of {[Fe($\mathbf{L_1}$)$_2$](**4**)}$_2$·H_2O·MeOH were grown by vapour diffusion of diethyl ether into the reaction solution. The complex crystallised in the

triclinic space group *P*-1 and contained two complete molecules of [Fe($\mathbf{L_1}$)$_2$](**4**) one full occupancy water, as well as one full occupancy methanol. Additional solvent is present within the structure however, a satisfactory disorder model for the solvent was not found. As such the OLEX^2 Solvent Mask routine was used to mask the disordered electron density that correlates to approximately three diethyl ether molecules per cell. The two Fe(III) centres are both indicative of LS Fe(III) and are similar to those observed in the previous structures (Table 1). Interestingly one of the ligand molecules in one of the complexes is disordered over two sites with relative occupancies of 0.7 and 0.3 and one of the anions also contains a two site partial positional disorder with the same relative occupancies. Interestingly, and similarly to [Fe($\mathbf{L_1}$)$_2$](**2**), there are no obvious π-based interactions to the naphthalimides and the majority of crystal packing interactions involve hydrogen-bonding interactions (Fig. S49) between the metal complexes and anions. Therefore, it appears that the position of the sulfonate group (*i.e.* when in the 3-phenyl or 2-naphthyl positions) heavily influences the packing interactions. In this instance the lack of π-based interactions means the long range ordering does not display the same layering topologies as seen previously (Fig. 12).

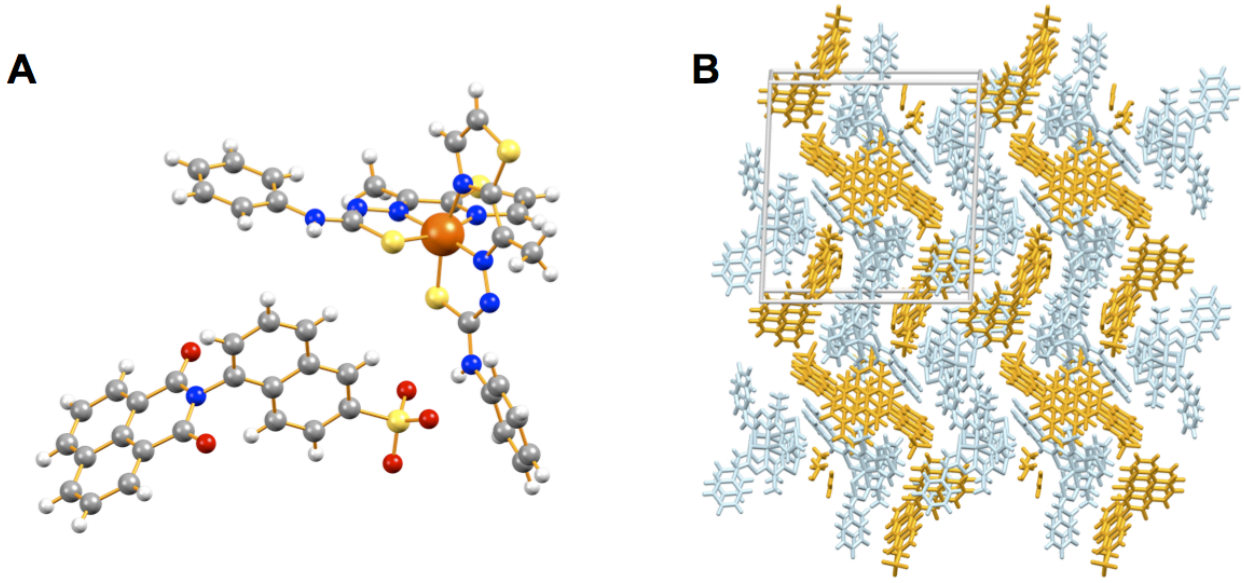

Figure 12: Ball and stick representation of the molecular structure of $\{[Fe(\mathbf{L_1})_2](\mathbf{4})\}_2 \cdot H_2O \cdot MeOH$ (**A**). Only the non-disordered independent molecule is shown and interstitial solvent molecules and lowest site occupancy disorder omitted for clarity. [Color scheme: Fe = Orange; S = Yellow; O = Red; N = Blue; C = Grey; H = White.] Overall packing (**B**) in $\{[Fe(\mathbf{L_1})_2](\mathbf{4})\}_2 \cdot H_2O \cdot MeOH$ [metal complex in blue and naphthalimde anion in orange].

A small number of small, poor quality, dark red plate-like single crystals of $[Fe(\mathbf{L_1})_2](\mathbf{5}) \cdot 2C_{16}H_{33}OH \cdot 2H_2O$ were grown by evaporation of the methanolic filtrate after isolation of the bulk sample from the diffusion of diethyl ether. It is important to note that the composition of this crystal is not representative of the bulk, in that the crystal obtained contains hexadecanol (presumably form the decomposition of hexadecyl sulfonate either during formation of the starting "iron(III)-hexadecylsulfonate" salt or during formation of the complex with $\mathbf{L_1}$) whereas the analysis of the bulk sample obtained *via* vapor diffusion of diethyl ether did not contain hexadecanol molecules. $[Fe(\mathbf{L_1})_2](\mathbf{5}) \cdot 2C_{16}H_{33}OH \cdot 2H_2O$ crystallized in the triclinic space group *P*-1 and contained one molecule in the asymmetric unit, two hexadecanol molecules and two

interstitial water molecules (Fig. 13). Again the Fe(III) cation is similar to the previous structures, Σ = 73.3°, (Table 1). Crystal packing is similarly controlled by hydrogen-bonding interactions between the metal complex and the anion *via* water molecules. Additionally, the presence of two hexadecanol molecules in the asymmetric unit also aid in the packing through hydrogen bond formation and interdigitation of the long alkyl chains (Fig. 14).

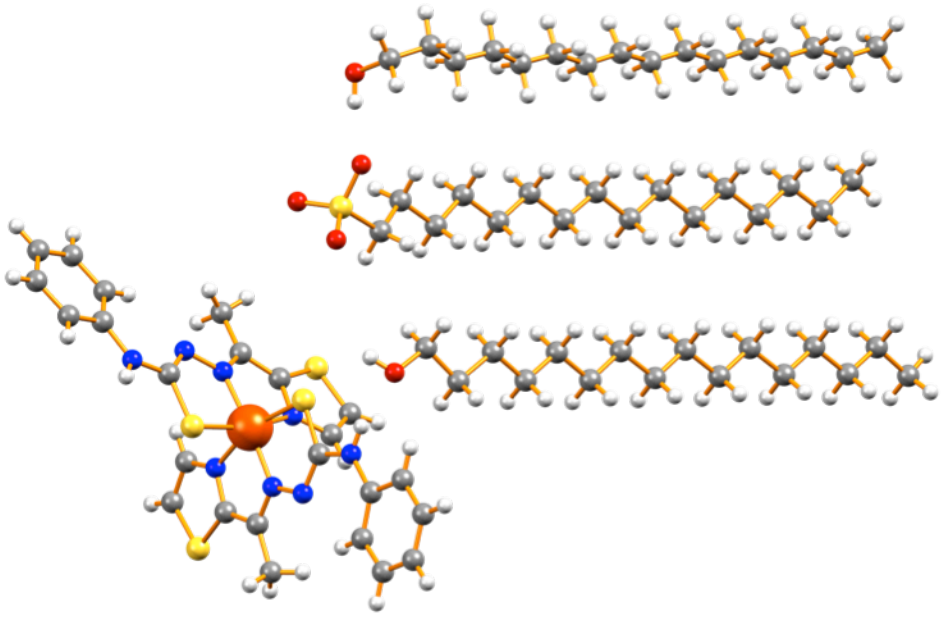

Figure 13: Ball and stick representation of the molecular structure of [Fe($\mathbf{L_1}$)$_2$](**5**)·2$C_{16}H_{33}OH$·2H_2O. Interstitial water molecules omitted for clarity. [Color scheme: Fe = Orange; S = Yellow; O = Red; N = Blue; C = Grey; H = White.]

The thioamine NH, from the metal complex, interacts with an oxygen donor atom on one hexadecanol [N1···O101 = 2.816(9) Å and ∠(N-H···O) = 168°], which in turn links to a water molecule [O101···O501 = 2.618(10) Å and ∠(O-H···O) = 168°]. The same water molecule (O501) acts as an H-bond acceptor to both another water molecule, [O501···O401 = 2.797(10) Å and ∠(O-H···O) = 159°], and to the hexadecylsulfonate anion [O501···O201 = 2.833(10) Å and ∠(O-

H···O) = 170°]. This sulfonate oxygen atom, O201, links to a second metal complex molecule via the thioamine NH of an alternate ligand around the metal centre, [N21···O201 = 2.878(9) Å and ∠(N-H···O) = 147°]. Another sulfonate oxygen atom, O203, acts as an H-bond donor in an interaction to the second hexadecanol molecule [O301···O203 = 2.667(10) Å and ∠(O-H···O) = 169°] (Fig. 14). Interestingly, the hydrophobic alkyl chains are oriented in one direction and interdigitate with neighbouring alkyl chains to form a bi-layer of amphiphilic components. This layered arrangement is similar to other reports of long-alkyl chain anion complexes.[54, 55]

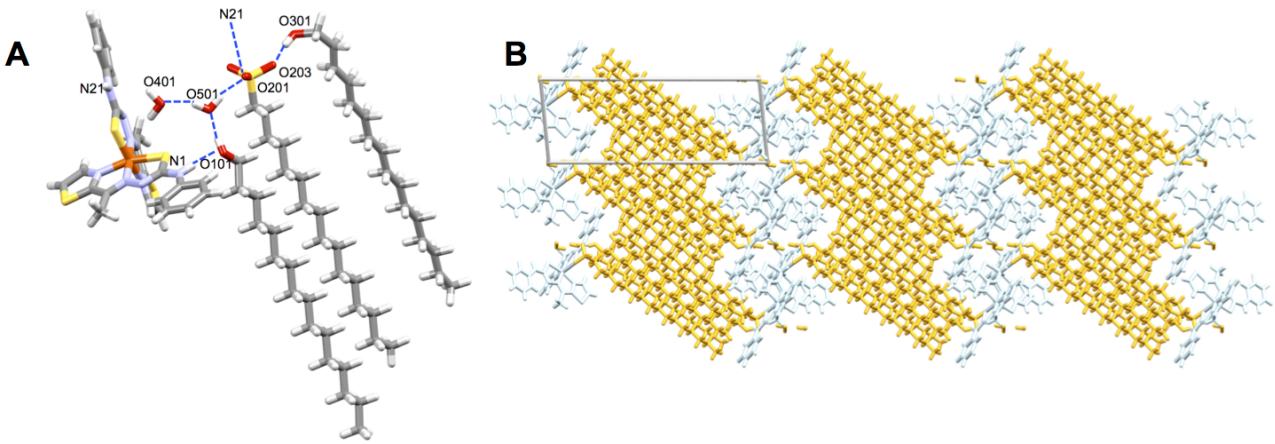

Figure 14: Hydrogen bonding interactions (**A**) present in the solid-state structure of [Fe($\mathbf{L_1}$)$_2$](**5**)·2$C_{16}H_{33}OH$·2H_2O. Overall packing showing interdigitation of alkyl chains to give bi-layers of metal complex (in blue) and amphiphiles (orange) (**B**). H-bonding shown by blue dashed lines: [N1···O101 = 2.816(9) Å and ∠(N-H···O) = 168°; O101···O501 = 2.618(10) Å and ∠(O-H···O) = 168°; O501···O401 = 2.797(10) Å and ∠(O-H···O) = 159°; O501···O201 = 2.833(10) Å and ∠(O-H···O) = 170°; N21···O201 = 2.878(9) Å and ∠(N-H···O) = 147°; O301···O203 = 2.667(10) Å and ∠(O-H···O) = 169°].

Overall, the crystallographic analysis of the complexes shows that by inclusion of the large organic sulfonate anions we are able to alter the extended structures compared to our previously reported complex $[Fe(\mathbf{L_1})_2](NO_3)$.[44] Specifically, the inclusion of 1,8-naphthalimide anions can give rise to the formation of layered structures. Additionally, the inclusion of a long chain sulfonate anion also gives rise to ordered layers of molecules that adopt a bi-layer arrangement in the solid-state. From these studies it is clear that the inclusion of structure directing anions influences the long range ordering of the Fe(III) thiosemicarbazone complex.

Langmuir film formation studies of $[Fe(\mathbf{L_1})_2](\mathbf{5})\cdot\mathbf{H_2O}$. Complex $[Fe(\mathbf{L_1})_2](\mathbf{5})\cdot H_2O$, with the inclusion of an amphiphilic anion into the structure, was designed for the formation of ordered mono-layers deposited onto a solid support using the Langmuir-Blodgett (LB) technique. Metal-based systems that introduce amphiphilicity into the complex through anion choice have been reported previously.[56-59] In order to investigate the suitability of $[Fe(\mathbf{L_1})_2](\mathbf{5})\cdot H_2O$ for the formation of immobilized mono-layers, a full study of the Langmuir film forming abilities at an air-water interface, was performed. Pressure area isotherms showed that, on pure water, $[Fe(\mathbf{L_1})_2](\mathbf{5})\cdot H_2O$ forms an ordered monolayer at the air-water interface with an area/chain value of 42 $Å^2$ and a film collapse pressure of 32 mNm^{-1} (Fig. 15(a)). However, stability measurements indicated that the film was unstable, as the measured surface pressure decreased by a factor of two, relative to the starting target surface pressure of 28 mNm^{-1}, over a period of two minutes (Fig. 15(b)).

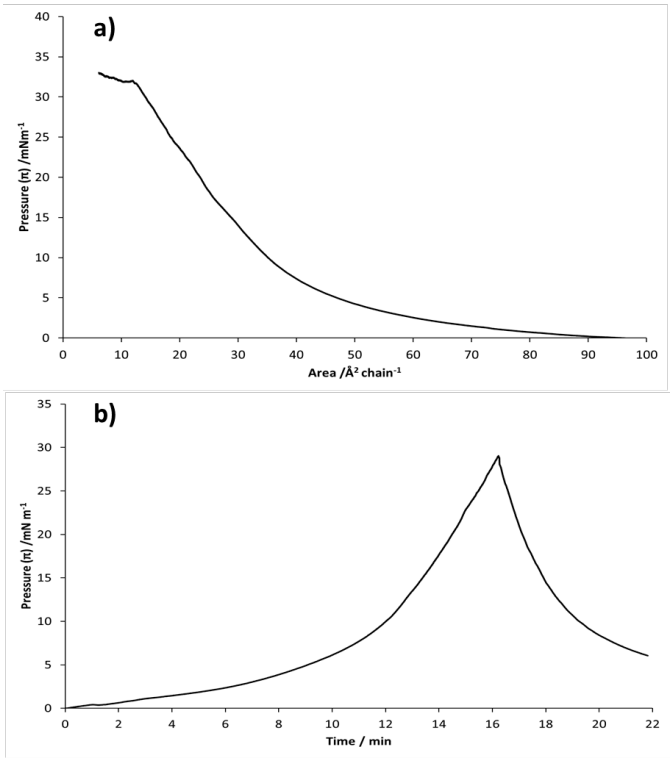

Figure 15: (a) [Fe($\mathbf{L_1}$)$_2$](**5**)·H_2O on water sub-phase formed a liquid compressed monolayer with an area per chain value of 42 Å^2/chain and underwent film collapse at 32 mNm^{-1}. **(b)** Stability experiment highlighting the instability of a liquid compressed monolayer of [Fe($\mathbf{L_1}$)$_2$](**5**)·H_2O formed at a surface pressure of 28 mNm^{-1}.

With the film formation and stability not suitable for LB deposition on water, the sub-phase was modified in order to attempt to give a stable monolayer of [Fe($\mathbf{L_1}$)$_2$](**5**)·H_2O. When using a sub-phase of NaCl (sat. aq.), the film was significantly more stable than when using pure water (Fig. 16) and allowed for deposition onto a quartz substrate.

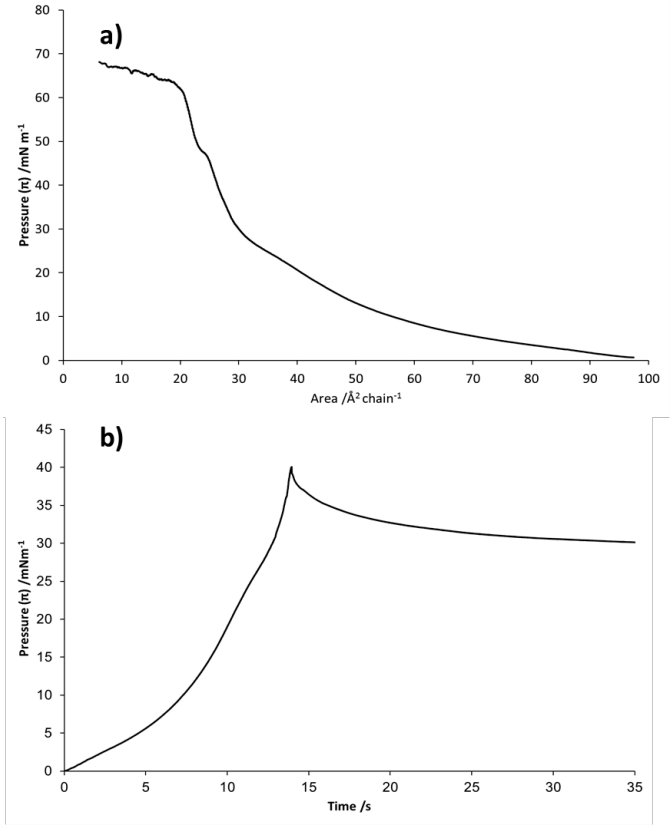

Figure 16: (a) [Fe($\mathbf{L_1}$)$_2$](**5**)·H_2O on NaCl (sat. aq.) sub-phase formed a liquid compressed monolayer with an area per chain value of 38 Å^2 chain^{-1} and underwent film collapse at 47 mNm^{-1}. **(b)** Stability experiment highlighting the stability of a liquid compressed monolayer of [Fe($\mathbf{L_1}$)$_2$](**5**)·H_2O formed at a surface pressure of 40 mNm^{-1}.

Upon emersion of the hydrophobic quartz substrate from the NaCl (sat. aq.) sub-phase, with the monolayer at the interface of the air and sub-phase, immobilization of the [Fe($\mathbf{L_1}$)$_2$](**5**)·H_2O complex on the surface was achieved (Fig. S44). However, a transfer ratio of ~2 was observed indicating partial film collapse during transfer of the monolayer to the substrate, as evidenced by the non-linear response. UV-visible spectroscopy measurements (Fig. 17) revealed that the complex was partially immobilized onto the surface of the substrate.

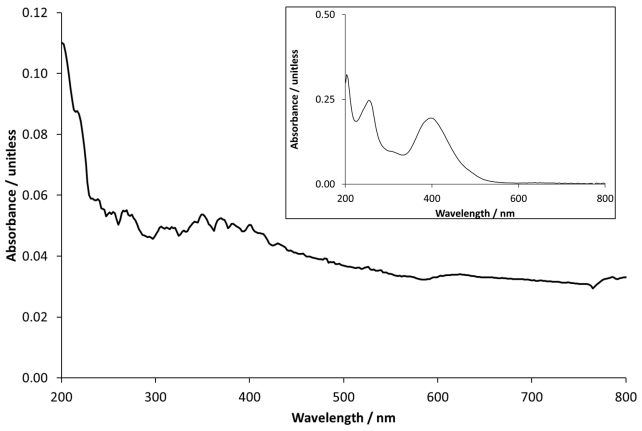

Figure 17: UV-visible transmission spectrum of [Fe($\mathbf{L_1}$)$_2$](**5**)·H_2O complex immobilized on a hydrophobic quartz substrate by the Langmuir-Blodgett technique, demonstrating absorbance features that correspond to absorbance features of the complex in the solution phase (inset).

Transfer of the [Fe($\mathbf{L_1}$)$_2$](**5**)·H_2O complex onto a substrate was achieved, which demonstrates the ability of anions to impart the desired functionality (*i.e.* amphiphilicity) into complexes for the formation of Langmuir-Blodgett films of potentially magnetically interesting complexes.

CONCLUSIONS

We have reported the synthesis and characterization of a family of 1,8-naphthalimide containing sulfonate anions and their subsequent inclusion into thiosemicarbazone-based Fe(III) complexes. Given the proven ability of 1,8-naphthalimide derivatives to extend solid-state structures through π-based interactions (when incorporated into the ligand scaffolds of metal complexes), a structural investigation was undertaken in order to determine if the same structure directing nature is observed when naphthalimide moieties are introduced into complexes *via* the anions. In three of the four structurally characterized complexes that featured the naphthalimide anions the extended

structures display layered topologies where the anions interact with cations *via* H-bonding and, in most cases, π-stacking interactions. Such structure extension is important for the enhancement of cooperativity in potentially spin crossover based complexes, additionally the formation of layers might allow for the ordered immobilization of functional complexes into thin film layers on surfaces. In an attempt to introduce additional functionality for targeted application (*i.e.* to allow for the formation of LB films), the amphiphilic hexadecyl sulfonate anion was introduced into the Fe(III) complex. Langmuir studies revealed that on a pure water sub-phase the system did not form a stable Langmuir film. However, when the sub-phase was brine, a stable monolayer formed. Moreover, the ordered monolayer was transferred onto a quartz slide highlighting the ability of designer anions to introduce functionality into complexes. Overall, this study has highlighted the ability of functionality to be introduced into metal complexes through designer anions rather than the more typical route of designer ligands. The methods reported herein are synthetically simple and do not require the often lengthy synthetic strategies used to introduce structure directing groups into ligand scaffolds, therefore making this method ideal for supramolecular materials development. Furthermore, such an approach allows for a library of functional anions that can be incorporated into a large range of metal complexes, potentially allowing for the generation of multifunctional systems where the anion plays an integral part in the structure and ordering of the system. The simplicity of our approach towards introducing structure-directing agents into coordination complexes potentially opens access to a vast range of novel metallosupramolecular materials where functional metal complexes can be organized into layered materials and/or deposited onto surfaces for potential application.

ASSOCIATED CONTENT

Supporting Information. The supporting Information is available free of charge on the ACS Publications website. The following files are available free of charge. NMR spectra (^{1}H and ^{13}C-NMR), IR spectra, UV/vis spectra, Fluorescence spectra, Additional crystallographic information. All data supporting this study are openly available from the University of Southampton repository.

AUTHOR INFORMATION

Corresponding Author

*j.a.kitchen@soton.ac.uk

Author Contributions

The manuscript was written through contributions of all authors. All authors have given approval to the final version of the manuscript.

Funding Sources

The authors are grateful to the University of Southampton for support of this work. We thank the EPSRC for funding through grant references EP/K039466/1, EP/N009185/1 & EP/K014382/1; the Royal Society for an Infrastructure grant to purchase a Langmuir Trough; and The Leverhulme Trust for the award of a Study Abroad Studentship to ABC.

ABBREVIATIONS

SDG, Structure Directing Group; LB, Langmuir-Blodgett; SBU, Secondary Building Unit.

References

1. *Functional Metallosupramolecular Materials*. Royal Society of Chemistry: Cambridge, 2015.
2. Duke, R. M.; Veale, E. B.; Pfeffer, F. M.; Kruger, P. E.; Gunnlaugsson, T. Colorimetric and fluorescent anion sensors: an overview of recent developments in the use of 1,8-naphthalimide-based chemosensors. *Chem Soc Rev* **2010**, 39, 3936-3953
3. Kurth, D. G. Metallo-supramolecular modules as a paradigm for materials science. *Sci. Tech. Adv. Mater.* **2008**, 9, 014103.
4. Pfeffer, F. M.; Buschgens, A. M.; Barnett, N. W.; Gunnlaugsson, T.; Kruger, P. E. 4-Amino-1,8-naphthalimide-based anion receptors: employing the naphthalimide N–H moiety in the cooperative binding of dihydrogenphosphate. *Tet. Lett.* **2005**, 46, 6579-6584.
5. Brooker, S.; Kitchen, J. A. Nano-magnetic materials: spin crossover compounds vs. single molecule magnets vs. single chain magnets. *Dalton Trans.* **2009**, 36, 7331-7340.
6. Jobe, K.; Brennan, C. H.; Motevalli, M.; Goldup, S. M.; Watkinson, M. Modular 'click' sensors for zinc and their application *in vivo*. *Chem. Commun.* **2011**, 47, 6036-6038.
7. Jiao, D.; Biedermann, F.; Tian, F.; Scherman, O. A. A Systems Approach to Controlling Supramolecular Architecture and Emergent Solution Properties via Host−Guest Complexation in Water. *J. Am. Chem. Soc.* **2010**, 132, 15734-15743.
8. Resnati, G.; Boldyreva, E.; Bombicz, P.; Kawano, M. Supramolecular interactions in the solid state. *IUCrJ* **2015**, 2, 675-690.
9. Busseron, E.; Ruff, Y.; Moulin, E.; Giuseppone, N. Supramolecular self-assemblies as functional nanomaterials. *Nanoscale* **2013**, 5, 7098-7140.
10. Saalfrank, R. W.; Uller, E.; Demleitner, B.; Bernt, I. In *Molecular Self-Assembly Organic Versus Inorganic Approaches*; Fuiita, M., Ed.; Springer Berlin Heidelberg: Berlin, Heidelberg, 2000; Vol. 96, pp 149-175.
11. Zhou, H.-C.; Long, J. R.; Yaghi, O. M. Introduction to Metal–Organic Frameworks. *Chem. Rev.* **2012**, 112, 673-674.
12. Wales, D. J.; Kitchen, J. A. Surface-based molecular self-assembly: Langmuir-Blodgett films of amphiphilic Ln(III) complexes. *Chem. Cent. J.* **2016**, 10:72.
13. Kitchen, J. A.; Barry, D. E.; Mercs, L.; Albrecht, M.; Peacock, R. D.; Gunnlaugsson, T. Circularly polarized lanthanide luminescence from Langmuir-Blodgett films formed from optically active and amphiphilic Eu(III)-based self-assembly complexes. *Angew. Chem. Int. Ed.* **2012**, 51, 704-708.
14. Barry, D. E.; Kitchen, J. A.; Albrecht, M.; Faulkner, S.; Gunnlaugsson, T. Near Infrared (NIR) Lanthanide Emissive Langmuir–Blodgett Monolayers Formed Using Nd(III) Directed Self-Assembly Synthesis of Chiral Amphiphilic Ligands. *Langmuir* **2013**, 29, 11506-11515.
15. Galanti, A.; Kotova, O.; Blasco, S.; Johnson, C.; Peacock, R. D.; Mills, S.; Boland, J.; Albrecht, M.; Gunnlaugsson, T. Exploring the Effect of Ligand Structural Isomerism in Langmuir-Blodgett Films of Chiral Luminescent EuIII Self-Assemblies. *Chem. Eur. J.* **2016**, 22, 9709-9723.
16. Keene, T. D.; Hursthouse, M. B.; Price, D. J. Stabilization of Discrete $[Cu(C_2O_4)_2(H_2O)_2]^{2-}$ Dianions in the Solid State by an Extensive Hydrogen Bonded Network. *Z. Anorg. Allg. Chem.* **2004**, 630, 350-352.

17. Keene, T. D.; Hursthouse, M. B.; Price, D. J. Two-Dimensional Metal−Organic Frameworks: A System with Competing Chelating Ligands. *Cryst. Growth Des.* **2009**, 9, 2604-2609.
18. Keene, T. D.; Rankine, D.; Evans, J. D.; Southon, P. D.; Kepert, C. J.; Aitken, J. B.; Sumby, C. J.; Doonan, C. J. Solvent-modified dynamic porosity in chiral 3D kagome frameworks. *Dalton Trans.* **2013**, 42, 7871-7879.
19. Keene, T. D.; Murphy, M. J.; Price, J. R.; Sciortino, N. F.; Southon, P. D.; Kepert, C. J. Multifunctional MOFs through CO_2 fixation: a metamagnetic kagome lattice with uniaxial zero thermal expansion and reversible guest sorption. *Dalton Trans.* **2014**, 43, 14766-14771.
20. Aguilera-Sigalat, J.; Bradshaw, D. A colloidal water-stable MOF as a broad-range fluorescent pH sensor *via* post-synthetic modification. *Chem. Commun.* **2014**, 50, 4711-4713.
21. Gasa, T. B.; Valente, C.; Stoddart, J. F. Solution-phase counterion effects in supramolecular and mechanostereochemical systems. *Chem. Soc. Rev.* **2011**, 40, 57-78.
22. Wang, Y.; Qi, W.; Huang, R.; Su, R.; He, Z. Counterion-Directed, Structurally Tunable Assembly of Hydrogels, Membranes, and Sacs at Aqueous Liquid-Liquid Interfaces. *Adv. Mater. Interf.* **2016**, 3, 1500327.
23. Wu, G.; Verwilst, P.; Liu, K.; Smet, M.; Faul, C. F. J.; Zhang, X. Controlling the self-assembly of cationic bolaamphiphiles: counterion-directed transitions from 0D/1D to exclusively 2D planar structures. *Chem. Sci.* **2013**, 4, 4486-4493.
24. Faul, C. F. J.; Antonietti, M. Ionic Self-Assembly: Facile Synthesis of Supramolecular Materials. *Adv. Mater.* **2003**, 15, 673-683.
25. Martinez, C. R.; Iverson, B. L. Rethinking the term “pi-stacking”. *Chem. Sci.* **2012**, 3, 2191-2201.
26. Gilday, L. C.; Robinson, S. W.; Barendt, T. A.; Langton, M. J.; Mullaney, B. R.; Beer, P. D. Halogen Bonding in Supramolecular Chemistry. *Chem. Rev.* **2015**, 115, 7118-7195.
27. Cavallo, G.; Metrangolo, P.; Milani, R.; Pilati, T.; Priimagi, A.; Resnati, G.; Terraneo, G. The Halogen Bond. *Chem. Rev.* **2016**, 116, 2478-2601.
28. Reger, D. L.; Elgin, J. D.; Semeniuc, R. F.; Pellechia, P. J.; Smith, M. D. Directional control of π-stacked building blocks for crystal engineering: the 1,8-naphthalimide synthon. *Chem. Commun.* **2005**, 4068-4070.
29. Reger, D. L.; Debreczeni, A.; Reinecke, B.; Rassolov, V.; Smith, M. D.; Semeniuc, R. F. Highly Organized Structures and Unusual Magnetic Properties of Paddlewheel Copper(II) Carboxylate Dimers Containing the π−π Stacking, 1,8-Naphthalimide Synthon. *Inorg. Chem.* **2009**, 48, 8911-8924.
30. Reger, D. L.; Debreczeni, A.; Smith, M. D. Synthesis and structure of a zinc(II)-carboxylate trimer containing the π···π stacking, 1,8-naphthalimide synthon: A supramolecular metal–organic framework. *Inorg. Chim. Acta* **2010**, 364, 10-15.
31. Reger, D. L.; Semeniuc, R. F.; Elgin, J. D.; Rassolov, V.; Smith, M. D. 1,8-naphthalimide synthon in silver coordination chemistry: Control of supramolecular arrangement. *Cryst. Growth Des.* **2006**, 6, 2758-2768.
32. Reger, D. L.; Leitner, A.; Smith, M. D. Homochiral, Helical Coordination Complexes of Lanthanides(III) and Mixed-Metal Lanthanides(III): Impact of the 1,8-Naphthalimide Supramolecular Tecton on Structure, Magnetic Properties, and Luminescence. *Cryst. Growth Des.* **2015**, 15, 5637-5644.

33. Kitchen, J. A.; Zhang, N.; Carter, A.; Fitzpatrick, A. J.; Morgan, G. G. Structural and magnetic properties of dinuclear Cu(II) complexes featuring triazolyl-naphthalimide ligands. *J. Coord. Chem.* **2016**, 69, 2024-2037.
34. Hawes, C. S.; Byrne, K.; Schmitt, W.; Gunnlaugsson, T. Flexible Porous Coordination Polymers from Divergent Photoluminescent 4-Oxo-1,8-naphthalimide Ligands. *Inorg. Chem.* **2016**, 55, 11570-11582.
35. Kitchen, J. A.; Martinho, P. N.; Morgan, G. G.; Gunnlaugsson, T. Synthesis, crystal structure and EPR spectroscopic analysis of novel copper complexes formed from *N*-pyridyl-4-nitro-1,8-naphthalimide ligands. *Dalton Trans.* **2014**, 43, 6468-6479.
36. Lovitt, J.; Hawes, C.; Lynes, A.; Haffner, B.; Möbius, M.; Gunnlaugsson, T. Coordination chemistry of *N*-picolyl-1,8-naphthalimides: colourful low molecular weight metallo-gelators and unique chelation behaviours. *Inorg. Chem. Front.* **2017**, 4, 296-308.
37. Clemente-León, M.; Coronado, E.; Soriano-Portillo, A.; Mingotaud, C.; Dominguez-Vera, J. M. Langmuir–Blodgett films based on inorganic molecular complexes with magnetic or optical properties. *Adv. Colloid Interfac.* **2005**, 116, 193-203.
38. Zhang, R.-J.; Liu, H.-G.; Si, Z.-K.; Zhu, G.-Y.; Zhang, H.-W. Fabrication and fluorescence characterization of the LB films of luminous rare earth complexes $Eu(TTA)_3Phen$ and $Sm(TTA)_3Phen$. *Thin Solid Films* **1997**, 295, 228-233.
39. Pavier, M. A.; Richardson, T.; Searle, T. M.; Huang, C. H.; Zhou, D. Photoluminescence study of Langmuir-Blodgett films of a hemicyanine molecular complex containing Yb^{3+}. *Supramol. Sci.* **1997**, 4, 437-441.
40. Adati, R. D.; Pavinatto, F. J.; Monteiro, J. H. S. K.; Davolos, M. R.; Jafelicci, M.; Oliveira, O. N. Synthesis of a functionalized europium complex and deposition of luminescent Langmuir–Blodgett (LB) films. *New J. Chem.* **2012**, 36, 1978-1984.
41. van Koningsbruggen, P. J.; Maeda, Y.; Oshio, H. Iron(III) Spin Crossover compounds. *Top. Curr. Chem.* **2004**, 233, 259-324.
42. Howe, E. N. W.; Busschaert, N.; Wu, X.; Berry, S. N.; Ho, J.; Light, M. E.; Czech, D. D.; Klein, H. A.; Kitchen, J. A.; Gale, P. A. pH-Regulated Nonelectrogenic Anion Transport by Phenylthiosemicarbazones. *J. Am. Chem. Soc.* **2016**, 138, 8301-8308.
43. Zhao, X.-H.; Zhang, S.-L.; Shao, D.; Wang, X.-Y. Spin Crossover in $[Fe(2\text{-Picolylamine})_3]^{2+}$ Adjusted by Organosulfonate Anions. *Inorg. Chem.* **2015**, 54, 7857-7867.
44. Laverick, R. J.; Carter, A. B.; Klein, H. A.; Fitzpatrick, A. J.; Keene, T. D.; Morgan, G. G.; Kitchen, J. A. Synthesis and characterisation of Fe(III) and Co(III) complexes of thiazole-containing thiosemicarbazone ligands. *Inorg. Chim. Acta* **2017**, 463, 126-133.
45. Coles, S. J.; Gale, P. A. Changing and challenging times for service crystallography. *Chem. Sci.* **2012**, 3, 683-689.
46. CrystalClear-SM Expert 3.1. (Rigaku: 2012).
47. CrysAlisPro 38.41, (Rigaku Oxford Diffraction, 2015).
48. Sheldrick, G. M. A short history of *SHELX*. *Acta Crystallogr. A* **2008**, 64, 112-122.
49. Dolomanov, O. V.; Bourhis, L. J.; Gildea, R. J.; Howard, J. A. K.; Puschmann, H. *OLEX2*: a complete structure solution, refinement and analysis program. *J. App. Cryst.* **2009**, 42, 339-341.
50. Labit, H.; Goldar, A.; Guilbaud, G.; Douarche, C.; Hyrien, O.; Marheineke, K. A simple and optimized method of producing silanized surfaces for FISH and replication mapping on combed DNA fibers. *BioTechniques* **2008**, 45, 649-658.
51. Drew, M. G.; Harding, C. J.; McKee, V.; Morgan, G. G.; Nelson, J. Geometric control of manganese redox state. *Chem. Commun.* **1995**, 1035–1038.

52. Miller, R. G.; Brooker, S. Spin Crossover, Reversible Redox, and Supramolecular Interactions in 3d Complexes of 4-(4-Pyridyl)-2,5-dipyrazyl-pyridine. *Inorg. Chem.* **2015**, 54, 5398-5409.
53. Feltham, H. L. C.; Klöwer, F.; Cameron, S. A.; Larsen, D. S.; Lan, Y.; Tropiano, M.; Faulkner, S.; Powell, A. K.; Brooker, S. A family of 13 tetranuclear zinc(II)-lanthanide(III) complexes of a [3 + 3] Schiff-base macrocycle derived from 1,4-diformyl-2,3-dihydroxybenzene. *Dalton Trans.* **2011**, 40, 11425-11432.
54. Kitchen, J. A.; White, N. G.; Jameson, G. N. L.; Tallon, J. L.; Brooker, S. Effect of Counteranion X on the Spin Crossover Properties of a Family of Diiron(II) Triazole Complexes $[Fe^{II}_2(PMAT)_2](X)_4$. *Inorg. Chem.* **2011**, 50, 4586-4597.
55. White, N. G.; Feltham, H. L. C.; Gandolfi, C.; Albrecht, M.; Brooker, S. Towards Langmuir–Blodgett films of magnetically interesting materials: solution equilibria in amphiphilic iron(II) complexes of a triazole-containing ligand. *Dalton Trans.* **2010**, 39, 3751-3758.
56. Byrd, H.; Whipps, S.; Pike, J. K.; Ma, J.; Nagler, S. E.; Talham, D. R. Role of the template layer in organizing self-assembled films: zirconium phosphonate monolayers and multilayers at a Langmuir-Blodgett template. *J. Am. Chem. Soc.* **1994**, 116, 295–301.
57. Seip, C. T.; Granroth, G. E.; Meisel, M. W.; Talham, D. R. Langmuir-Blodgett films of known layered solids: Preparation and structural properties of octadecylphosphonate bilayers with divalent metals and characterization of a magnetic Langmuir-Blodgett film. *J. Am. Chem. Soc.* **1997**, 119, 7084–7094.
58. Wu, A.; Talham, D. R. Photoisomerization of Azobenzene Chromophores in Organic/Inorganic Zirconium Phosphonate Thin Films Prepared Using a Combined Langmuir−Blodgett and Self-Assembled Monolayer Deposition. *Langmuir* **2000**, 16, 7449-7456.
59. Fabre, R. M.; Talham, D. R. Stable Supported Lipid Bilayers on Zirconium Phosphonate Surfaces. *Langmuir* **2009**, 25, 12644-12652.

For Table of Contents Only

Investigating the Structure Directing Properties of Designer 1,8-Naphthalimide and Amphiphilic Sulfonate Anions and their Fe^{III} Thiosemicarbazone Complexes

*Anthony B. Carter, Robert J. Laverick, Dominic J. Wales, Sarah O. Akponasa, Aaron J. Scott, Tony D. Keene and Jonathan A. Kitchen**

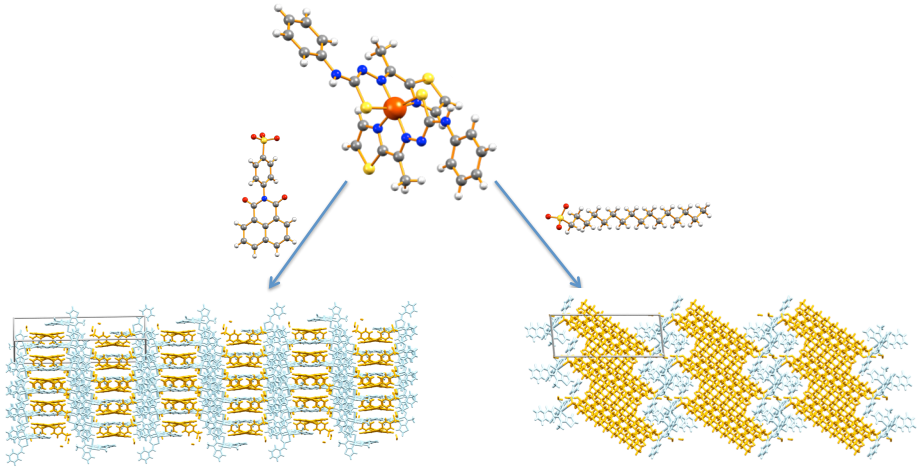

Synopsis

A series of Fe^{III} thiosemicarbazone complexes featuring novel 1,8-naphthalimide sulfonate-based anions was prepared and the structure directing properties investigated. The designer naphthalimide-based anions show interesting structure extension though π-stacking in the solid state. In addition a long chain sulfonate anion was incorporated to introduce amphiphilicity to the complex and allow for formation of Langmuir-Blodgett films.